AD_____

Award Number: W81XWH-07-1-0159

TITLE: Identification and Therapeutic Targeting of Paracrine Senescence Factors in the Prostate Tumor Microenvironment

PRINCIPAL INVESTIGATOR: James P. Dean, M.D., Ph.D.

CONTRACTING ORGANIZATION: Fred Hutchinson Cancer Research Center
Seattle, WA 98109-1024

REPORT DATE: October 2011

TYPE OF REPORT: Final

PREPARED FOR: U.S. Army Medical Research and Materiel Command
Fort Detrick, Maryland 21702-5012

REPORT DOCUMENTATION PAGE

Form Approved
OMB No. 0704-0188

1. REPORT DATE	2. REPORT TYPE	3. DATES COVERED
October 2011	Final	1 March 2007 – 16 September 2011

4. TITLE AND SUBTITLE

Identification and Therapeutic Targeting of Paracrine Senescence Factors in the Prostate Tumor Microenvironment

5a. CONTRACT NUMBER

5b. GRANT NUMBER
W81XWH-07-1-0159

5c. PROGRAM ELEMENT NUMBER

6. AUTHOR(S)

James P. Dean, M.D., Ph.D.

E-Mail: amoreno@fhcrc.org

5d. PROJECT NUMBER

5e. TASK NUMBER

5f. WORK UNIT NUMBER

7. PERFORMING ORGANIZATION NAME(S) AND ADDRESS(ES)

Fred Hutchinson Cancer Research Center
Seattle, WA 98109-1024

8. PERFORMING ORGANIZATION REPORT NUMBER

9. SPONSORING / MONITORING AGENCY NAME(S) AND ADDRESS(ES)
U.S. Army Medical Research and Materiel Command
Fort Detrick, Maryland 21702-5012

10. SPONSOR/MONITOR'S ACRONYM(S)

11. SPONSOR/MONITOR'S REPORT NUMBER(S)

12. DISTRIBUTION / AVAILABILITY STATEMENT
Approved for Public Release; Distribution Unlimited

13. SUPPLEMENTARY NOTES

14. ABSTRACT

The goal of this proposal was to examine the induction of senescence by common effective treatments for prostate cancer, and to further identify and target senescence-associated factors which might mediate resistance to these therapies in the neoplastic epithelium. Senescence cell biomarkers (p16 and DcR2) were correlated with with aging and prostate cancer. The senescence-associated factors GDF15 and STC1 were found to correlate with neoplasia, but not aging. Stressful environmental conditions leading to altered secretion of STC1 were defined, but multiple studies seeking to define the function of STC1 in the prostate were uniformly negative. A clinical trial testing the effects of neoadjuvant anti-IGF-1R (IMC-A12) treatment in combination with androgen deprivation was completed and a panel of serum biomarkers were evaluated. We find biomarker evidence for good on-target efficacy and an intriguing correlation of PSA response with A12-induced insulin resistance that is not fully accounted for by pre-treatment factors such as body mass index.

15. SUBJECT TERMS
Prostate, cancer, senescence, paracrine, resistance, chemotherapy, androgen deprivation, stanniocalcin 1, STC1, IGF-1R, insulin resistance, IMC-A12, neoadjuvant, biomarker

16. SECURITY CLASSIFICATION OF:			17. LIMITATION OF ABSTRACT	18. NUMBER OF PAGES	19a. NAME OF RESPONSIBLE PERSON
					USAMRMC
a. REPORT	b. ABSTRACT	c. THIS PAGE			19b. TELEPHONE NUMBER *(include area code)*
U	U	U	UU	67	

Table of Contents

Introduction

Deaths due to prostate cancer- the second leading cause of cancer death in men in the United States - could be prevented with more effective treatments. Overcoming tumor cell resistance to the effects of androgen deprivation and chemotherapies would significantly improve the morbidity and mortality of prostate cancer. We ***hypothesized*** that the induction of cellular senescence in the tumor microenvironment by androgen deprivation and cytotoxic chemotherapy promotes the resistance and survival of carcinoma cells. We further ***hypothesized*** that targeting senescence-associated pro-survival paracrine factors will enhance the effects of these therapies and enhance response and cure rates.

To address these hypotheses, we had three aims: First, to identify senescence changes in prostate tissue induced by androgen deprivation and chemotherapy, specifically focusing on identifying factors with the potential to influence the survival/resistance of neoplastic epithelium via paracrine mechanisms. Second, to evaluate the effects of inhibiting specific senescence-associated pro-survival factors using *in vivo* models. Third, to develop and execute clinical trials designed to inhibit senescence-associated paracrine survival mechanisms and determine if enhanced tumor responses can be achieved.

Body

The following summarizes the research accomplishments of this proposal, as associated with each task in the Statement of Work.

Technical Objective 1: To determine the effects of chemotherapy and androgen ablation therapy on the frequency, type, and location of senescent cells in the prostate, and to identify changes in levels of senescence-associated signaling molecules found in those tissues.

Objective 1a. *Identify senescent cells in pre- and post-chemotherapy prostate tissues from 58 patients.*

Task 1. Perform histochemical staining of a defined set of senescence biomarkers. (Months 1-6)

To complete this task, we employed a set of pre-treatment and post-chemotherapy tissues from a neoadjuvant clinical trial testing the effects of 3 months combined mitoxantrone and docetaxel chemotherapy treatment. To identify senescent cells in these post-treatment prostate tissues, we completed histochemical staining for the "gold standard" marker of senescence, Senescence-Associated β-Galactosidase (SA-β-Gal) on a random sample of 25 of the post-chemotherapy treated patients. We employed an assay optimized for maximal histochemical sensitivity and specificity.

We also established staining conditions for the immunohistochemical staining of two well-established biomarkers of senescence, p16(INK4a) and DcR2. To establish these conditions, antigen retrieval, blocking, titration of primary antibodies, and detection methods were optimized. These staining protocols were then employed to examine our Tissue Microarray of Aging and Prostate Cancer.

We developed and produced The Tissue Microarray of Aging and Prostate Cancer as a unique tissue microarray resource specifically for the purpose of examining the correlations of senescent cells and senescence-associated factors with aging in benign and neoplastic prostate tissues. This tissue microarray contains prostate tissue cores with benign and neoplastic epithelium from the prostatectomy blocks of 25 men aged less than fifty years old and 25 men aged greater than 70 years old, spotted in quadruplicate. Results of this staining are described below.

Task 2. Analyze stained tissues, quantitating frequency of positive staining cells in the epithelium versus stroma, in or near benign versus neoplastic prostate glands. (Months 2-8)

Of the 25 post-chemotherapy patient samples tested, only 6 had detectable SA-β-Gal staining. Staining intensity and localization was highly variable in these six. Only one sample had intense staining with the other five staining weakly. The localization of staining was primarily in microscopic prostate glands. Staining intensity within a positively-staining gland was generally homogeneous, but the distribution of positively-staining glands was extremely variable within the any given tissue section. For example, a given tissue section might have as few as zero positively staining glands per low power field in one area and up to 20 positively staining glands in another area. This lack of consistent, widespread distribution of staining posed significant limitations to our ability to pathologically evaluate and consistently quantitate relative levels of staining. In consultation with our collaborating genitourinary pathologist, Dr. Larry True, our judgement was that staining of the pre-treatment needle core biopsy tissues was unlikely to demonstrate statistically significant increases in staining after chemotherapy treatment. Thus, further SA-β-Gal staining was not pursued in these samples.

Staining for p16(INK4a) and DcR2 on the Tissue Microarray of Aging and Prostate Cancer was completed and assessed as described above. We quantitated the intensity and the frequency of staining in the benign epithelium, neoplastic epithelium, and the stroma, using a 0-2+ point scale for staining intensity, noting the percentage of cells in each compartment staining at each intensity level.

Task 3. Perform statistical analyses to determine the significance of staining differences between the various compartments and differences before and after chemotherapy. (Months 2-8)

DcR2 and p16(INK4a) staining scores were calculated for each sample by multiplying the percentage of cells at a given stain intensity level times the value of that staining level (0, 1+ or 2+). Staining scores were then subjected to standard statistical techniques to characterize each cellular compartment and differences between the various comparator groups.

This work demonstrated low levels of staining for p16(INK4a) in the benign epithelium and in the stroma (Table 1). In the benign epithelium, approximately 1-3% of the cells had identifiable staining, with an average staining level of 1+. In the stroma a similar number of cells, approximately 1-2%, stained positively for p16(INK4a) with average 1+ staining. In both compartments, aging was associated with increased staining (p-values of <0.05), but obviously positive-staining cells still represented rare events. By contrast, in the neoplastic epithelium, 1+ intense p16(INK4a) staining was much more frequent and seen in about 30% of the cells, but no difference was seen with between the young and aged cohorts.

Similar to the p16(INK4a) staining, the DcR2 biomarker of senescence also stained very few cells in the stroma (0.2-0.7%)(Table 1). With aging, there was a significant increase in the frequency of staining positivity (increase from 0.19 to 0.70, $p<0.05$). By contrast, staining in the neoplastic epithelium was dramatically more frequent, with 88-97% of cells staining positive for

DcR2. However, despite (or perhaps as a result) of the high levels of staining, there was no significant increase with aging ($p=0.43$) in the neoplastic epithelium. Only in the benign epithelium was there a significant increase in DcR2 staining seen with aging. This difference in benign epithelium was quantitatively substantial in addition to being statistically significant. In the young cohort, 16.5% of cells stained positively, compared to 39% of cells in the aged cohort ($p<0.0001$).

Therefore, consistent with our prediction, we find increased numbers of senescent cells that in the benign epithelium and stromal compartments in aged men, when compared to young men (Table 1). The magnitude of increased p16(INK4a) and DcR2 staining ranges from 2.3 to 3.7-fold more staining in aged men, compared to young men. There are also highly significant increases in the staining scores of the neoplastic epithelium compared to the benign epithelium, irrespective of patient age for both of these markers (p-values uniformly < 0.0001).

Overall with respect to the senescence biomarker staining, we have validated these staining protocols and these protein biomarkers as tools for the investigation of senescence in prostate tissues. We have also provided experimental evidence in the human prostate to support the long-standing hypothesis that chronological aging is correlated with increased senescence, specifically in the prostate. The finding of neoplasm-associated increases in these markers is novel and of uncertain significance.

Objective 1b. *Identify senescent cells in pre- and post-androgen ablation prostate tissues from 48 patients.*

Task 4. Perform histochemical staining of a defined set of senescence biomarkers. (Months 12-20) -

The tissues to be analyzed in this objective were to come from a clinical trial of neoadjuvant androgen ablation therapy given prior to prostatectomy. Ultimately due to poor accrual, one arm of the clinical trial was discontinued for a revised total enrollment goal of 36 patients. To ensure optimal results in analyses of these limited tissues, it was not possible to stain these tissues prior to initiation of other planned laboratory analyses. These analyses (outside the scope of this proposal) included frozen tissue sectioning and collection of laser-captured cells from benign, cancer, stroma in the pre- and post-treatment samples. This concurrent analysis was necessary primarily to preserve the limited tissue available and secondarily to allow comparison of senescence-associated-β-galactosidase staining (requiring frozen tissue sections) with the quantitative analysis of RNA gene expression levels for genes associated with senescence as defined in our previously published work (Bavik, et al, 2006, Coppe, et al, 2008), and that of others (Untergasser et al, 2002). Unfortunately, these concurrent analyses had not been initiated as of the end date of this grant and thus these tissues were not available for this histochemical staining.

Task 5. Analyze stained tissues, quantitating frequency of positive staining cells in the epithelium versus stroma, in or near benign versus neoplastic prostate glands. (Months 13-22)

Task 6. Perform statistical analyses to determine the significance of staining differences between the various compartments and differences before and after chemotherapy. (Months 13-22)

Objective 1c. *Examine senescence-associated signaling molecules in pre- and post-chemotherapy prostate tissues from 58 patients.*

Task 7. Perform histochemical staining of secreted signaling molecules. (Months 3-18)

a. Tissue Microarry of Aging and Prostate Cancer Immunostaining: As with the p16(INK4a) and DcR2 immunohistochemistry described above, we employed the tissue microarray of aging and prostate cancer to optimize the staining for a set of senescence-associated, secreted signaling molecules. Based on the proteomics data as discussed in the Preliminary Data of our grant and other unpublished work, we chose to investigate the staining of STC1, GDF15, CXCL1, IL8. In that work, this set of molecules had been identified and confirmed to be increased upon senescence induction of primary prostate stromal cells. Immunohistochemical staining was therefore optimized and completed on the tissue microarray of aging for STC1, GDF15, CXCL1 and IL8 proteins.

b. Post-chemotherapy Tissue Immunostaining: As described in the original proposal, one goal of this project was to examine prostate tissues for changes in senescence-associated signaling molecules after chemotherapy treatments. Based on the aging-associated differences in STC1 secretion levels identified in the Tissue Microarray of Aging and Prostate Cancer, we opted to examine STC1 levels in tissues from a cohort of patients treated with chemotherapy as described in Objective 1a. A total of 10 post-chemotherapy patient samples from this study were stained for STC1.

c. Rapid Autopsy Prostate Cancer Metastases Microarray Immunostaining: To further examine senescence changes in a more highly pre-treated population of prostate cancer patients, we also examined STC1 staining in a case series of metastatic prostate cancer tissues collected as part of a rapid autopsy program from men with end-stage, metastatic prostate cancer. These patients had been treated with a heterogeneous and diverse set of medical therapies for metastatic prostate cancer prior to their deaths, including hormonal therapies and chemotherapies. Thus, these tissues are a valuable resource for examining the combined effect of these therapies in patients with advanced disease. In particular, among the cores in this tissue microarray, 44 bony metastases were examined.

d. Consecutive Serial Section Immunostaining Co-localization: Given the interesting patterns and heterogeneity in prostatic stromal STC1 staining observed in the Tissue Microarray of Aging experiments, we completed an experiment using consecutive serial sections of a neoplastic prostate gland. Alternate serial sections were stained for STC1 and markers for various individual constituents of the stroma. Stromal constituents of interest included fibroblasts/myofibroblasts, endothelium, neurons, macrophages and dendritic cells. TE7, Caldesmon, Sm-a-actin, and Factor XIIIa were stained to identify possible fibroblastic and myofibroblastic cells. Neuronal cells were identified with Neurofilament and S100. Dendritic markers included CD21, CD35 and CD1a. Endothelium was stained with CD31 and CD34. Macrophages were stained with CD68.

e. Quantitative analysis of gene expression changes in Senescence-associated signaling molecules. Collaborators in the Nelson lab and elsewhere have identified a pattern of gene expression (Senescence-associated secretory proteins) that takes place as a consequence of chemotherapy treatment in prostate cancer tissues, as well as other cancers in vitro and in vivo. As an adjunct to the immunohistochemistry studies described above, and given the limitations of these studies, we analyzed the pre- and post-chemotherapy levels of these molecules in the tissues described in Objective 1a.

Task 8. Analyze stained tissues, quantitating staining intensities and locations of positive staining; epithelium versus stroma, in or near benign versus neoplastic prostate glands. (Months 4-20)

a. Tissue Microarray of Aging and Prostate Cancer: Despite optimization, CXCL2 and IL8 staining were not sufficiently intense for quantitation or further characterization by immunohistochemistry. The staining patterns of STC1 and GDF15 were analyzed similarly to the p16 and DcR2 analyses as described above. We quantitated the intensity and the frequency of staining in the benign epithelium, neoplastic epithelium, and the stroma, using a 0-2+ point scale for staining intensity, assigning percentage of cells stained at each intensity level. An example of this staining is shown in Figure 1. In the three sections shown, cells within Gleason Pattern 3 glands (arrow 1) nearly all show significant staining, with heterogeneity in staining intensity. There was variability to STC1 staining of neoplastic glands ranging from little to very intense. Presumably, this reflects either the inherent variability in the genetic states of different patient neoplasms and/or variability in senescence changes in different cancers.

By contrast, overall there was significantly less staining of STC1 in the benign epithelial glands. There was significantly more variability in the staining patterns compared to neoplastic glands with two patterns seen. One pattern was a more homogeneous low level (1+) staining throughout the glands of the core (arrows 2), and other pattern was a more focal and intense staining seen scattered in cells through the glands (arrow 3). This inconsistency is reflected in the approximately 50% decrease in staining score, reflecting the average amount of staining in benign glands compared to neoplastic glands.

Most intriguingly, there was a heterogeneity in stromal staining which was not as easily explained. Although fibroblastic and myofibroblastic stroma are presumed to comprise the majority of the stromal compartment, many other cell types may also be present permanently or transiently. In some cores, a more diffuse staining of the stroma can be appreciated (arrows 4), such as in the top and bottom panels of Figure 1. In other cores, such as the middle panel of Figure 1, there are very intense, individual cells that can be appreciated. Of the intensely staining cells in the stroma, several patterns can also be appreciated in the stroma. In some cases, clusters of intensely staining cells also have the morphological features of nerve bundles (arrow 5). Other cells had a linear appearance, possibly consistent with nerves or myofibroblasts (arrow 6). Finally, scattered cells with intense staining were more non-descript and could not be identified morphologically.

b. Post-chemotherapy prostate tissues: As described in the original proposal, one goal of this project is to examine prostate tissues for changes in senescence-associated signaling molecules after chemotherapy treatments. We applied the optimized protocol for STC1 as above to stain a limited set of post-chemotherapy prostate tissues. A total of 10 patient samples were stained for STC1. As with the SA-B-Gal staining described above, flash-frozen sections were employed in this study. This was necessary to allow possible comparisons with pre-treatment tissues. Representative photos of two patient samples from this study are shown in Figures 2 and 3. In each case, illustrative areas of STC1 staining were selected, with photos also taken of the corresponding area from these sections exposed to a non-immune antiserum as a negative control.

Figure 2, Panel A shows a homogeneous, lightly staining gland with little background in the negative control. The stroma also shows scattered cells staining intensely, in a background

of diffuse staining. However, in the stroma, the negative control shows similar diffuse staining of the stroma, albeit at lower intensity. Intensely staining stromal cells have a similar decreased intensity in the negative control. Panel B shows a single, intensely staining linear array of cells having the appearance of a nerve bundle. The remainder of the stroma was as described for Panel A.

Figure 3, Panel A shows the intense and specific staining that is associated with cell bundles having the appearance of nerve bundles. Diffuse staining with rare, scattered, intensely-staining cells can also be appreciated in the stroma. However, in comparison with the negative control, the staining in the stroma is quite equivocal. By contrast with the formalin-fixed, paraffin-embedded (FFPE) tissues of the TMA of aging, much less staining of benign epithelial glands could be appreciated in these frozen sections with a significant background in the negative control. In Panel B, numerous neoplastic epithelial glands are stained rather intensely with STC1. Similar to the staining in the stroma and the benign epithelium, there is also a significant amount of background staining seen in the negative control.

To sum, staining can be appreciated in the stroma, benign epithelium and neoplastic epithelium of these post-chemotherapy treated patients. However, unlike the FFPE staining achieved in the TMA of aging, there is a significant amount of background staining in all three compartments, despite optimization of the protocol. Despite optimization, this significantly limited the likelihood to detect specific and significant differences in STC1 staining as a function of chemotherapy treatment in the prostate.

c. Rapid Autopsy Prostate Cancer Metastases Microarray: As described above, a tissue microarray consisting of various metastatic prostate cancer tissues obtained from men by rapid autopsy shortly after death was stained for STC1. Forty-four cores in this microarray are composed of bony metastases, with the balance including lymph nodes, kidney and liver samples. A representative set of interesting STC1 staining patterns of these bony metastases are shown in Figure 4. In panel A, several scattered metastatic prostate glands are interspersed into a sparsely cellular stroma adjacent to bone. In panel B, more intensely staining glands are interspersed with an extensive amount of bone. In panel C, intensely staining hematopoietic bone marrow is seen as an aggregate from the 7 o'clock to the 2 o'clock position, with interspersed fat globules. A more lightly staining ovoid composed of prostate glands is seen centered on the 3 o'clock position. In panel D, two deposits of metastatic prostate cancer are surrounded by a sparsely cellular stroma, with a small focus of more intensely staining hematopoietic bone marrow at the 11 o'clock position. These results are representative of the staining seen in the bone samples of this TMA, and suggest that the staining seen in the primary tumors is retained during the metastatic process. Further exploratory analyses of the bone and soft tissue metastasis staining find no significant differences in STC1 staining when comparing untreated primary tumors (as assessed in the Tissue Microarray of Aging and Prostate Cancer) with these treated Rapid Autopsy microarray samples, suggesting that stable levels of STC1 expression are not significantly altered in post- chemotherapy tissues and nor as a function of metastatic tumor microenvironment.

d. Consecutive Serial Section Immunostaining Co-localization: As described above, we completed an experiment using consecutive serial sections of a neoplastic prostate gland, interspersing STC1-stained sections with staining for various other likely and interesting possible constituents of the stroma. No significant co-localization could be appreciated for dendritic markers including CD21, CD35 and CD1a, the macrophage marker CD68, the endothelial mark-

ers CD31 and CD34, or the fibroblastic/myofibroblastic markers TE7 and Factor XIIIa. By contrast, clear co-localization was demonstrated for the neuronal markers Neurofilament and S100, as well as the fibroblastic/myofibroblastic markers Caldesmon and Sm-a-actin.

Seen in Figures 5 and 6, the flanking STC1-stained sections are the top and bottom panels, with STC1-positive cell examples highlighted by the arrowheads. In the middle, staining for Caldesmon (Figure 5) and Sm-a-actin (Figure 6) is shown of intervening sections, with the similar cells also highlighted by the arrowheads. These data first demonstrate that the majority of the stromal compartment is comprised of fibroblastic/myofibroblastic cells. Although not surprisingly given the ubiquity of these cells in the stroma, reasonable evidence is found for co-localization of STC1-staining cells with these two stains. This suggests that STC1 may be staining a minor sub-set of the fibroblastic stroma, perhaps the part which has undergone senescence. The lack of significant co-localization with the TE7 and Factor XIIIa staining is not surprising, as these markers are not ubiquitous through the stroma, but are only found to stain minor subsets of the fibroblastic/myofibroblastic stroma.

Staining of Neurofilament (Figure 7) and S100 (Figure 8) was even clear. Highly intense staining bundles of cells are seen in the STC1-stained panels at the top and bottom of each figure (arrows), while the intervening sections respectively stained for these neuronal markers co-localize with similarly intense staining of these cellular bundles. This even more unequivocally demonstrates that the nerves of the prostate are intensely stained with STC1 and retrospectively, identifies similar intensely-staining cell bundles in the TMA of aging and the post-chemotherapy tissues as almost certainly neuronal in origin. Other data, not shown, demonstrates that some of the intensely-staining linear cells as seen in the middle panel of Figure 1, are also likely neuronal in origin.

Task 9. Perform statistical analyses to determine the significance of staining differences between the various compartments and differences before and after chemotherapy. (Months 4-20) Analyses failed to demonstrate any age-dependent changes in the staining intensities, frequencies, or patterns for the GDF15 or STC1 proteins ($p=0.09-0.97$)(Table 1). For GDF15, there is a statistically significant increase in the staining of neoplastic compared to benign epithelium in both young men ($p<0.0001$) and old ($p<0.0001$). In the case of STC1, only the young men have a statistically significant increase in the staining of neoplastic epithelium ($p<0.005$). No significant stromal GDF15 staining was visualized. By contrast, the increased STC1 staining seen in the stroma with aging bordered on the statistically significant ($p=0.09$). In fact, STC1 is the first protein we have examined with intense and widespread stromal staining patterns.

Optimized protocols for IL8 and CXCL1 failed to yield staining that could be analyzed in a meaningful fashion.

Qualitative interpretations of the staining results are as described above.

Objective 1d. *Examine senescence-associated signaling molecules in pre- and post-androgen ablation prostate tissues from 48 patients.*

Task 10. Perform histochemical staining of secreted signaling molecules. (Months 12-36)

See above outcome as described in Objective 1b.

Task 11. Analyze stained tissues, quantitating staining intensities and locations of positive staining; epithelium versus stroma, in or near benign versus neoplastic prostate glands. (Months 13-36)

See above outcome as described in Objective 1b.

Task 12. Perform statistical analyses to determine the significance of staining differences between the various compartments and differences before and after chemotherapy. (Months 13-36)

See above outcome as described in Objective 1b.

Objective 1e. *Correlate observed senescence staining results from Objectives 1a-1d with clinical outcomes and gene expression data.*

Task 13. Collate senescence staining results and clinical outcomes. (Months 4-40)

Due to the histochemical and immunohistochemical staining limitations, correlation with clinical outcomes were not possible.

Task 14. Collaborate with Nelson laboratory members performing the parallel expression studies to correlate staining patterns with gene expression changes. (Months 4-40)

In a complementary approach to the histochemical and immunohistochemical studies described above, we performed quantitative real-time PCR experiments on RNA isolated from the pre- and post-chemotherapy treated tissues of the clinical trial described in Objective 1a. Laser capture microscopy was first used to isolate cells from each of the three tissue compartments of interest: neoplastic epithelium, benign epithelium, and stroma. After amplification, quantitative real-time PCR was used to assay changes in expression levels of senescence biomarkers, as well as senescence-associated secreted proteins.

Quantitative analysis of gene expression changes in Senescence-associated signaling molecules. Quantitative real-time analyses of a panel of senescence-associated secretory proteins was performed using primer sets shown to be specific for the gene messages. The cycle threshold was quantitated using standard methods, and normalized to RPL13a gene levels for each sample. The normalized values were then compared between pre-chemotherapy and post-chemotherapy samples. These demonstrated substantial increases in many, although not all of the investigated molecules. These changes were completely consistent with induction of senescence as a result of chemotherapy treatment in human tissues.

We have demonstrated statistically significant increases ranging from 3.7- to 28-fold in the expression of the senescence biomarkers p16 and p21 in all three compartments of the prostate, as a result of chemotherapy treatment (Figure 9 and Coppe et al, 2008). CXCL1 (GROa) and IL8, investigated as described above in Objective 1c, also had statistically significant increases in gene expression (from 2.6- to 22-fold) in all three compartments after chemotherapy treatment. In addition, MMP3 and IGFBP2 were among the senescence-related proteins identified in our Preliminary data mass spectrometry experiments and were found to have increased expression after chemotherapy treatment (1.4- to 36-fold increase) in these analyses (Figure 9 and Coppe et al, 2008).

<u>Characterization of prostatic STC1 in vitro and in vivo</u>

Given the sum of data suggesting the relevance of senescence in response to chemotherapy and the significant effects of senescence, aging, neoplasia, and chemotherapy treatment on STC1, we

opted to understand the importance of this protein, previously uncharacterized in the prostate and never associated with prostate cancer.

STC1 gene expression increases in the prostate after chemotherapy treatment for prostate cancer

Given the difficulty of using immunohistochemistry to characterize changes in STC1 after chemotherapy treatment as described above, laser capture microdissection was used to capture cells from the tissues of the clinical trial described in Objective 1a. Cells were captured from each of three cellular compartments of the prostate- stroma, benign epithelium, and neoplastic epithelium. Isolated and amplified RNA was reverse transcribed and used in a quantitative real-time PCR assay to quantitate levels of STC1 gene expression in these samples.

Normalized to the RPL13a housekeeping gene, there were clearly changes in STC1 gene expression after chemotherapy treatment with the combination of docetaxel and mitoxantrone, particularly in the benign epithelium where a nearly 60-fold average increase in STC1 expression was seen ($p<0.01$) (Figure 10). Increased STC1 was also seen in the stroma (6-fold), but it was not statistically significant ($p<0.08$) due to inter-patient variability. Interestingly, when comparing the pre-chemotherapy tissues with one another, the neoplastic epithelium had the highest basal expression of STC1, followed by the stroma, then the benign epithelium (Figure 10). This is in contrast to the immunohistochemistry STC1 protein localization data detailed above and may represent the limitations of the in vitro models currently available or variable correlation between STC1 RNA levels and protein secretion levels in vivo.

<u>STC1 secretion is increased by a broad and diverse spectrum of stressful microenvironmental conditions</u>

Given the differences between the immunohistochemistry and gene expression quantitation, it was apparent that STC1 secretion in the prostate needed to be fully characterized to allow further studies.

In the literature, numerous growth conditions have been previously found to induce STC1 secretion in various tissues, but prostate tissues and cell lines had never been tested. Consistent with published literature, STC1 secretion from prostate stromal cells was induced by hypoxia (1% oxygen, compared to normoxia - 20% oxygen) (Figure 11b), calcium (but not magnesium) (Figure 12a), phosphate (but not sulfate) (Figure 12b), and osmotic stress (sodium chloride) (Figure 12c). For each of these factors, there was a concentration-dependence for each of these treatments. Calcium, phosphate and osmotic stress treatments were subsequently shown to at least additively increase STC1 secretion under hypoxic conditions as well as normoxic conditions.

Interestingly, we discovered that serum was the most effective inductive factor (Figure 11a, data not shown), in both normoxic and hypoxic conditions. A titration of serum concentrations demonstrated that STC1 secretion was dose-dependent (Figure 13). To further characterize the serum-dependent STC1 secretion changes, cells were treated with increasing amounts of serum which had been pre-treated by boiling. Compared to unboiled serum control, there were slight decreases in STC1 secretion induced by boiled serum (Figure 13). This suggested that there were heat labile factors (such as proteins) which contribute to increased STC1 secretion, but non-heat-labile factors account for the majority of the serum effect. Given the effects of osmotic stress, calcium and phosphate on STC1 secretion, these likely account for some, if not all the non-heat-labile effects. Together, these experiments suggested that STC1 secretion may play

a central role in responses to diverse alterations in environmental conditions, particularly abnormal or stressful conditions.

Given our initial identification of STC1 as a factor with secretion increased by senescence, we also tested various forms of senescence induction in prostate stromal cells (Figure 14). It is notable that the induction of senescence takes place under cellular stress. In addition to oxidative stress (hydrogen peroxide); direct DNA damage (bleomycin exposure), replicative exhaustion (telomere exhaustion) (Figure 14a), and oncogene-induced senescence (RAS overexpression) result in increased STC1 secretion levels. In contrast, p16 overexpression (direct induction of senescence) (Figure 14b) did not result in increased STC1 expression. Thus, increased STC1 secretion is a largely, although not wholly, generalized response to stressful, senescence-inducing conditions.

To identify which cellular signaling pathways which might be important for increased levels of STC1 secretion, we tested the effects of several small molecule inhibitors of cellular signaling cascades (Figure 15). Particularly in the case of the mitogen-activated protein kinase pathway inhibitor UO126, there was a dose-dependent inhibition of the STC1 secretion induced by serum. This inhibition was also seen to a lesser extent for the protein kinase A pathway inhibitor H89 and the phosphatidyl inositol-3-kinase pathway inhibitor LY294002. This suggests that all three pathways play a role in the STC1 secretion increases, with the MAPK pathway being most important. However, perhaps even more interestingly, induction - rather than inhibition- of STC1 secretion could be seen for intermediate doses of H89 and LY294002. Thus, the data for these inhibitors in the presence of serum can not be interpreted simply, but must take into account this mixed picture of inhibition plus induction.

Given the possibility that STC1 appears to be secreted in response to cellular stress, specific doses of these drugs may be sufficient to induce the secretion of STC1 in some circumstances as a non-specific stress effect.

Prior work by Gerritson et al had suggested hepatocyte growth factor (HGF) might specifically induce increased STC1 secretion from endothelial cells. Although our early work suggested that this mechanism was also intact in prostate stromal cells, this was subsequently found to not be reproducible. As part of this work, the small kinase inhibitor SU11274 was employed in an attempt to specifically inhibit downstream signaling from the HGF receptor c-met. Not only did this inhibitor not reduce STC1 secretion, it actually induced STC1 secretion (Figure 16a) in a dose-dependent fashion (Figure 16b). This was consistent with the inductive effects of the other signaling cascade inhibitors described above and further supports a model where inhibition of the important c-met pathway induces cellular stress, thus increasing STC1 secretion.

Perhaps most importantly, given the data from our immunohistochemistry and gene expression studies of STC1 changes after clinical chemotherapy treatment of prostate cancer, we tested whether STC1 secretion from the stromal cells was altered by docetaxel, mitoxantrone, or bleomycin (Figure 17). Indeed, we found STC1 to be induced by ongoing docetaxel and bleomycin chemotherapy treatments (distinguishable from the post-bleomycin senescent cells discussed above), but not mitoxantrone.

As noted, all of the above studies were performed on prostate stromal cell lines, where this factor was originally identified. To more fully understand the interplay of the stroma and epithelium in the prostate tissue, we tested four independent prostate epithelial cell lines representing benign epithelium (Primary epithelial cells- PECs), androgen-dependent epithelium (LNCaP), and castration-resistant epithelium (PC3) cells for STC1 secretion. Interestingly, STC1 could only be detected in the conditioned medium of PC3 cells (Figure 18), even after 10-

fold concentration and exposure of the other cell types to the above-defined inducing conditions (data not shown). However, in the PC3 cells, significantly less STC1 is secreted, compared to secretion levels of stromal cells.

There are also similarities and differences noted in the inducing conditions. For example, hypoxia induces PC3 STC1 secretion but there is less effect of osmotic stress induced by sodium chloride (Figure 18). Calcium may have caused cell death as it resulted in no detectable STC1. However, the effect of sodium phosphate was pronounced in both serum-free and normal serum conditions. By contrast with stromal cells, both mitoxantrone and docetaxel both induce STC1 secretion from PC3 cells. However, the SU11274 c-met inhibitor only induced STC1 under serum-free conditions in PC3 cells.

STC1 effects on Proliferation

The effects of exogenous STC1 on proliferation of LNCaP, Du145 and PC3 cells were also tested. Replicate wells were plated with 5000 cells of each respective cell line either in serum-free media or media containing 10% serum. Subsequently, recombinant purified STC1 (BioVendor Research and Diagnostics Products) or purified goat-anti-STC1 polyclonal antibody (R and D Systems) were added to final concentrations of 0.5 ug/ml or 2 ug/ml, respectively. In addition, ATP signaling has been shown to be affected by STC1 (Block et al, 2010), thus the effects of ATP were tested at final concentrations of 50 or 500 μM, alone and in combination with STC1. Finally, the purified goat-anti-HGF polyclonal antibody (R and D Systems) was used as a control for antibody addition at final concentration of 2 ug/ml. In this fashion the effects of increased STC1 and the effects of decreased/neutralized STC1 were tested. After 3 days of incubation with daily addition of ATP, cell numbers were quantitated with an MTS assay (Promega). As seen in Figure 19, the effects of exogenous STC1 and STC1 neutralization with or without ATP addition were not statistically significant compared to relevant internal controls under serum-free conditions for BPH1, Du145 and PC3 cell lines. Similar results were obtained when cells were treated and grown in 10% serum. Effects were similar across replicate experiments.

STC1 effects on growth under hypoxic conditions

Given the significant induction of STC1 in prostate stromal and PC3 cell lines grown under hypoxic conditions, as well as other stress-inducing environmental conditions, I hypothesized that STC1 might be acting as a survival factor. To test this, recombinant human STC1 or anti-STC1 antibodies as described above were added to replicate wells plated to hold 5000 LNCaP, Du145 or PC3 cells. Duplicate plates were placed into standard atmospheric oxygen-containing incubators or a 1% oxygen-containing hypoxia incubator, respectively. At various time points, plates were removed and cell numbers quantitated using an MTS assay (Promega). Cell proliferation effects under normoxic conditions were as seen in Figure 1 (data not shown). Seen in Figure 20, there were clear effects of hypoxia on cell viability over time in all three cell lines. Contrary to prediction, there was no statistically significant effect consistent with STC1 increase by addition of recombinant protein and decrease by anti-STC1 antibody.

STC1 effects on Chemotherapy Response

To evaluate the effects of STC1 supplementation or neutralization on chemotherapy resistance and/or sensitivity, replicate wells were plated with 5000 cells of the BPH1, LNCaP, Du145, or PC3 cell lines. Six hours later, STC1 and control treatments were started as per proliferation experiments above. Twenty-four hours after plating, cells began treatment with vary-

ing concentrations of docetaxel (0-100 nM) or mitoxantrone (0-800 nM) based on IC50 values previously determined for the PC3 cell line of 10 and 100 nM, respectively. Cell numbers were quantitated using the MTS assay (Promega) after 3 days of treatment. No significant effects of STC1 supplementation or neutralization could be discerned in any of the four cell lines relative to internal controls (Du145 not shown) upon docetaxel treatment (Figure 21). Mitoxantrone responses were similarly not significant (data not shown).

STC1 effects on cell motility/wound healing

A wound-healing or "scratch" assay was used to examine the contribution of STC1 to cell motility. Briefly, equal numbers of cells were plated and 24 hours later, a sterile pipet tip was used to denude a zone on the cell culture plate of cells. BPH1, Du145 (data not shown) and PC3 cells were each tested. Wells were treated to supplement or neutralize endogenous STC1 as detailed above. Reference marks were made and photographs of the identical locations were taken at multiple time points after denudation. The distance between the two masses of cells were measured on the resulting photographs and graphed over time. STC1 supplementation and neutralization had no significant or reproducible effect on epithelial cell migration compared to appropriate control conditions (Figure 22). Additional variables tested but not displayed for graph clarity included serum-free conditions, ATP treatment alone or combined with STC1.

STC1 effects on intracrine androgen metabolism

In the ovarian system, STC1 treatment of ovarian granulosa cells suppresses production of progesterone and its metabolic enzymes (Luo et al, 2004). In the prostate, our group (Montgomery et al, 2008) and others (Titus et al, 2005) have demonstrated the persistence of intratumoral androgens and have implicated tumoral steroid hormone metabolic enzyme changes in this process. Given the importance of testosterone in prostate cancer etiology and treatment, I sought to characterize whether STC1 might modulate intratumoral production of androgens. To evaluate this, RNA was purified from the LNCaP, PC3 and Du145 cell lines. Validated quantitative real-time PCR primers were obtained from Dr. Elahe Mostaghel in the Nelson laboratory and used to quantitate changes in the various enzymes known to participate in the interconversion of androgens and their steroid precursors (Figure 23). As predicted, the PC3 and Du145 (data not shown) cell lines generally express much higher levels of these enzymes, as predicted by the castration resistant state of these lines, compared to the androgen-dependence of LNCaP. Unfortunately, STC1 supplementation and neutralization were associated with maximal changes in these enzymes of 25% or less (data not shown), suggesting minimal, if any role for STC1 in these changes.

In Summary, these studies thoroughly identified changes in stromal secretion of STC1 upon alteration of environmental conditions with a broad spectrum of factors, including hypoxia, calcium, phosphate, osmotic stress, and serum (which was persistent even with boiled serum). Multiple methods of senescence induction were found to increase STC1 secretion, including oxidative stress (hydrogen peroxide), direct DNA damage (bleomycin exposure), replicative exhaustion (telomere exhaustion), oncogene overexpression (RAS), but not direct but not direct p16-induced induction of senescence. Cellular treatment with small molecule inhibitors of second messenger signaling systems yielded a mixed picture of induction and inhibition, likely due to the combination of stress response induction and specific pathway inhibition. In particular, the MAPK pathway appeared to be particularly important in mediating STC1 secretion. In contrast

with endothelial cells, HGF did not significantly alter STC1 secretion while specific inhibition of the c-met receptor for HGF was actually found to increase STC1 secretion. Dynamic treatments with some chemotherapies (docetaxel and bleomycin) but not mitoxantrone increased STC1 secretion. Finally, STC1 was found to be only minimally secreted from PC3 cells, but not from LNCaP nor primary prostate epithelial cells. This was significantly different from the results seen with prostate tissue staining where the epithelium had the highest levels of STC1 and the stroma was lower.

Unfortunately, in functional studies, only the most modest, if any effects were seen on modulation of STC1 in the microenvironment. No consistent or reproducible effects were seen on proliferation, tolerance of hypoxia, resistance or sensitivity to chemotherapy, cell motility/wound healing or intracrine androgen metabolism.

Technical Objective 2. To examine resistance of senescence-induced carcinogenesis and tumor progression to the effects of docetaxel and/or the anti-IGF-IR antibody IMC-A12 in a nude mouse xenoplant model.

Objective 2a. *Obtain regulatory approval for animal xenoplant trials.*

Task 15. Write animal protocol for therapy trials. (Months 1-2).

This was completed as described in prior annual reports.

Task 16. Obtain necessary animal review board approval. (Months 2-5).

Fred Hutchinson Cancer Research Center Institutional Animal Care and Use Committee approval was obtained for the proposed studies (IACUC #1743). USAMRMC Animal Care and Use Review Office (ACURO) approval was also obtained as described in prior annual reports.

Objective 2b. *Determine the resistance of senescent-dependent carcinogenesis and early tumors to docetaxel chemotherapy.*

Task 17. Culture cells and prepare cellular recombinants with BPH1 or PC3 and primary prostate stromal cells, senescent, or not. Perform sub-kidney capsule implantation surgeries. After 2 weeks of recovery, treat mice with weekly docetaxel for 3 weeks. 2 months after completion of therapy, sacrifice mice and retrieve xenoplanted kidneys. (Months 5-12)

The experimental work proposed in this Objective, as with Objectives 2c and 2d were repeatedly deferred to allow commitment of time and energies into work on the other two Objectives in this grant. However, a small series of studies designed to complement this work was completed. In these studies, we demonstrated that replicative senescence, as well as senescence induced by hydrogen peroxide, is capable of mediating the growth stimulatory effects in nude mouse kidney capsule xenograft models as previously described in the grant proposal. Secondly, we demonstrated that the NPF prostate stromal cell line, in addition to the PSC27 and PSC36 cell lines, is capable of mediating senescence-dependent growth stimulation. The results of these experiments confirm the consistency of prostate stromal senescence-dependent epithelial stimulation.

Task 18. Measure resulting graft sizes, fix and embed the tissues, then stain with Hematoxylin and Eosin and immunohistochemistry. Evaluate for invasiveness, senescent cell populations and neoplastic morphologies. (Months 8-14)

As per Task 17.

Task 19. Perform statistical analyses to determine significance of chemotherapy-induced changes in the senescent-stimulated, compared to the pre-senescent recombinants. (Months 10-16)

As per Task 17.

Objective 2c. *Determine the effect of IMC-A12 on senescent-dependent carcinogenesis and early tumors.*

Task 20. Culture cells and prepare cellular recombinants with BPH1 or PC3 and primary prostate stromal cells, senescent, or not. Perform sub-kidney capsule implantation surgeries. After 2 weeks of recovery, treat mice with thrice weekly IMC-A12 injections continuously for 2 months, then sacrifice mice and dissect out kidneys. (Months 7-12).

As per Task 17.

Task 21. Measure resulting graft sizes, fix and embed the tissues, then stain with Hematoxylin and Eosin and immunohistochemistry. Evaluate for invasiveness, senescent cell populations and neoplastic morphologies. (Months 10-14)

As per Task 17.

Task 22. Perform statistical analyses to determine significance of chemotherapy-induced changes in the senescent-stimulated, compared to the pre-senescent recombinants. (Months 12-18)

As per Task 17.

Objective 2d. *Determine the senescence-dependent resistance of advanced tumors to docetaxel chemotherapy and its modulation by IMC-A12.*

Task 23. Culture cells and prepare cellular recombinants with BPH1 or PC3 and primary prostate stromal cells, senescent, or not. Perform sub-kidney capsule implantation surgeries. Two months after implantation, treat mice with weekly docetaxel for 3 weeks, with or without IMC-A12 thrice weekly treatments. 3 weeks after completion of therapy, sacrifice mice and dissect out kidneys. (Months 10-18).

For further details please see explanation under Objective 2b, Task 17.

Task 24. Measure resulting graft sizes, fix and embed the tissues, then stain with Hematoxylin and Eosin and immunohistochemistry. Evaluate for invasiveness, senescent cell populations and neoplastic morphologies. (Months 13-20)

As per Task 17.

Task 25. Perform statistical analyses to determine significance of chemotherapy-induced changes in the senescent-stimulated, compared to the pre-senescent recombinants. (Months 15-22)

As per Task 17.

Technical Objective 3: To develop and execute clinical trials evaluating the effectiveness of inhibiting senescence-associated modulators of cancer cell survival in the treatment of prostate cancer. The lead candidate for such targeting is currently IGF1R in the insulin-like growth factor pathway. Other targets identified in Specific Aims/Technical Objectives 1 and 2 may also present opportunities for treatment of more novel targets. Optimal target selection and clinical trial design will be determined during year 2 of the proposal.

Objective 3a: *Participate in the execution and analysis of a Phase II clinical trial inhibiting senescence-associated modulators of cancer cell survival in combination with androgen ablation in the neoadjuvant setting prior to radical prostatectomy. The lead class of modulators are anti-IGF1R antibodies under development by Imclone (IMC-A12) or Pfizer (CP-751,871) which inhibit the insulin-like growth factor pathway. Other candidates/pathways will be considered and optimized during the clinical trial design phase of the project in year 2.*

Task 26. Design Clinical Trial (Months 15-18)

As part of the educational program detailed in my proposal, I attended the 2007 ASCO/AACR Methods in Clinical Cancer Research workshop, July 27-August 3, 2007, during which time I had the opportunity to further refine the proposed clinical trial as detailed above. Subsequent to this, a Food and Drug Administration Investigational New Drug application was submitted and duly approved (IND 79729). The clinical trial was approved by the Scientific Review Committee of the Fred Hutchinson/University of Washington Cancer Consortium. Approval was subsequently obtained from the University of Washington Human Subjects Review Committee V (institutional review board) and the Fred Hutchinson/University of Washington Cancer Consortium Institutional Review Board.

Separately, in consultation with Ms. Johanna Kidwell of the Human Subjects Protection Office, Office of Research Protections at U.S. Army Medical Research and Material Command, we obtained local institutional review board approval and further HSPO/ORP approval prior to the planned laboratory investigations in the tissues from these patients. These approvals were obtained and subsequent USAMRMC ORP HRPO approval memorandum for the laboratory analyses was received on July 28, 2010, HRPO Log Number A-14104.4

In the clinical trial, 28 patients were treated with the Imclone anti-IGF-IR antibody IMC-A12 every two weeks simultaneously with combined androgen deprivation therapy (goserelin plus bicalutamide). After three months of this treatment, patients underwent standard open prostatectomy. Tissues excess to the needs of clinical pathological diagnosis and staging were collected to be analyzed for several laboratory endpoints, including gene expression changes and changes in cellular proteins by immunohistochemistry. All patients had pre-treatment prostate biopsy for the purposes of comparison with their prostatectomy tissues. The primary endpoint was pathological complete response rate (predicted to be 20%). This was to be compared to historical control data in which 5% of patients treated for 3 months with combined LHRH agonist and testosterone receptor antagonist prior to prostatectomy were found to have pathological complete response. This number of patients is calculated to provide 80% power to detect this difference with 5% one-sided Type I error rate.

Task 27. Develop recruitment materials, hold in-service for clinical providers and study coordinator. (Months 18-24).

Recruitment materials were limited to internet postings. As part of our University of Washington Human Subjects Review Committee application, a world-wide web-based recruitment posting was prepared. Once final approvals for the clinical trial were obtained, this was posted on the Fred Hutchinson/University of Washington Cancer Consortium, University of Washington Health Sciences and the Fred Hutchinson Cancer Research Center web sites. In addition, the study was posted on clinicaltrials.gov as required for all clinical trials.

I provided in-service training sessions to the University of Washington infusion center nursing staff, familiarizing them with the scientific rationale of the treatment, goals of the study, and the practicalities of administration and monitoring for unexpected or serious adverse events.

I have worked closely with the study coordinator in obtaining the IRB approvals. I also presented the clinical trial to physician providers and co-investigators.

Task 28. Recruit, enroll, and treat patients on study. Monitor and report adverse events. (Months 20-55)

Enrollment and treatment were completed as of June, 2011. There was one complete response. There were no serious or unexpected adverse events related to study treatment.

Task 29. Analyze pre- and post-treatment tissues for changes senescent cell content and senescence-associated signaling molecule expression as described above (Objectives 1a. and 1c.). (Months 24-46)

Analyses of the study sample tissues have been initiated. At the time of grant termination date, benign, cancer and stromal cell populations had been laser-captured from both biopsy and prostatectomy tissue samples of 14 patients. Separate monies from the PNW Prostate SPORE grant funding the parent clinical trial will be used in ongoing efforts to continue capture until complete sets of samples were available from all study patients. Gene expression will be quantitated and compared between the populations allowing treatment-specific gene expression changes to be identified, then compared and contrasted between the various tissue compartments.

Prior to grant termination, a study of the serum samples was completed analyzing changes in circulating biomarkers predicted to reflect the effects of A12 treatment in the first 18 consecutive accrued patients. Please see the section below for a complete discussion of the methods and results of this analysis.

Task 30. Collate and analyze data. (Months 24-50)

IGF-1R inhibition combined with Androgen Deprivation before prostatectomy for high risk prostate cancer: Serum biomarker evidence for on-target efficacy and novel correlation with PSA response.

Methods:

The clinical trial (A12) was designed to accrue 28 patients with localized prostate cancer who were at high risk for relapse after prostatectomy. The primary endpoint for the trial was pathological complete response (pCR) rate with this cohort size designed to provide 80% power to detect an increased pCR rate of 20%, compared to historical controls of 5% in trials of hormone therapy only. Treatment consisted of three months of treatment with goserelin (10.8 mg SQ once), bicalutamide (50 mg PO daily) and IMC-A12 (10mg/kg IV every 2 weeks). Tissue and serum acquisition was an integral component of trial design with pre-treatment serum collection as well as mandatory prostate biopsy for the sole purpose of research analyses. Serum samples were collected throughout treatment and at the time of prostatectomy. Prostate tissues excess to the needs of clinical diagnosis were collected at the time of prostatectomy. For the purposes of a control population, serum samples similarly collected in a concurrent clinical trial of neoadjuvant hormone therapy only (NeoADT) (detailed in Objectives 1b and 1d) were similarly analyzed. Pre-treatment values provided an internal control comparison.

Blood glucose, serum PSA and testosterone levels were measured in a CLIA-certified clinical pathology laboratory using certified methods. Commercial ELISA assays were used per manufacturer's instructions to assay the serum levels of human growth hormone (R and D systems), insulin (Invitrogen), and c-peptide of insulin (Diagnostic Systems Labs). Custom in-house ELISA assays were used to quantitate levels of IGF-I, IGF-II, IGFBP-3, and IGFBP-1 us-

ing the respective purified recombinant protein standards, monoclonal antibodies and biotinylated polyclonal antibodies from R and D systems. Samples were measured in duplicate and colorimetric methods used to quantitate protein levels versus a standard curve of purified standard protein. Inter- and intra-assay coefficients of variation ranged from 3-10% for these assays.

The clinical laboratory results and patient demographics were anonymized and linked with the research laboratory ELISA results by study personnel, then the linked data were subjected to further statistical and other analyses with as described below.

Results:

Cohort Demographics and Clinical Outcomes

As designed, the study accrued a population of prostate cancer patients at high risk of relapse after prostatectomy with median PSA of 12, diagnostic biopsy Gleason score of 4+4, and clinical stage of T2a (Table 2). The control population was designed to be a more intermediate-risk population and this is reflected in the lower PSA (5.2) and Gleason score (4+3). For later analyses, pre-treatment body mass index (BMI) becomes relevant and the two populations were of similar obesity and both on the borderline between "overweight" and "obese" as defined by the BMI.

Clinical pathological outcomes in this initial 18 patient cohort were limited to one complete response (Table 3). Tumor stage outcomes in the remaining patients corresponded to Kattan nomogram predictions (nomograms.org). In a similar fashion, the frequency of lymph node positivity was similar to Kattan nomogram predictions (6/18). Unfortunately, a substantial fraction of the patients (4/18) had positive surgical margins.

Grade 1 or 2 adverse events which were possibly or probably related to A12 therapy included 2 patients who required metformin therapy to treat significant treatment-induced hyperglycemia/diabetes (Table 3). Other grade 1 or 2 at least possibly related adverse events included skin rash, pruritis, dry skin, diarrhea, elevated aspartate transaminase, hypertension, increased lacrimation, blurry vision, scotomata, flashing lights, tinnitus, anemia, thrombocytopenia, and neutropenia. There were no probably or possibly related Grade 3 or 4 adverse events. Unrelated adverse events included peri-operative stroke, post-operative deep venous thrombosis with asymptomatic pulmonary embolism, and hypertension.

Effects of IMC-A12 plus hormonal therapy on IGF pathway homeostasis biomarkers: On-target efficacy

The IGF-1R is found in tissues throughout the body, including the pituitary. Normal homeostasis of the IGF pathway relies on feedback inhibition by IGF-I signaling through the pituitary IGF-1R (Gualberto et al, 2009). Loss of this feedback inhibition would be predicted to have effects on this homeostasis at multiple levels. As seen in Figure 24, upon IMC-A12 treatment, loss of this feedback inhibition leads to dramatically increased circulating levels of growth hormone compared to pre-treatment levels (8.1-fold, $p<0.002$) as well as the NeoADT cohort (3.3-fold, $p<0.004$). The predicted consequences of increased growth hormone include increases in IGF-I, IGF-II, IGFBP-3 and blood glucose levels. In fact, statistically significant increases are seen compared to pre-treatment levels and the hormone therapy-only cohort in IGF-I (3.1-fold $p<0.0001$, 4.5-fold $p<0.0001$), IGF-II (1.5-fold $p<0.006$, 1.9-fold $p<0.0001$) and IGFBP-3 (1.8-fold $p<0.003$, 1.9-fold $p<0.0001$). Together, these data strongly imply that IGF-1R signaling is being effectively inhibited by combination IMC-A12 with hormonal therapy in this patient population.

Effects of A12 plus hormonal therapy on glucose homeostasis biomarkers: Insulin resistance

Blood glucose is an additional factor predicted to be increased by elevated growth hormone levels. However, blood glucose increases are normally tightly controlled by secondary homeostatic mechanisms, including compensatory insulin increases. Clinically, elevations of blood glucose have been frequently observed in clinical trials across the various anti-IGF-1R therapeutics in development, including A12 (Gualberto et al, 2009). As seen in Figure 25, there are small and non-significant increases in blood glucose of approximately 15 points in the A12-treated patients, compared to pre-treatment values (1.15-fold $p=0.18$). Blood glucose is also increased compared to the NeoADT cohort (1.22-fold $p=0.11$). Notably, these were not fasting glucose levels and samples were not drawn at consistent times of the day relative to food ingestion patterns. Thus, these results should be considered with caution as a rough estimate of glucose alterations.

By contrast, insulin and its corresponding c-peptide of insulin were both much more substantially elevated (Figure 25). The elevations of insulin upon IMC-A12 treatment were non-significant due to high degrees of measurement variability, but were increased 3.8-fold compared to pre-treatment values ($p=0.19$) and 5-fold compared to the NeoADT cohort ($p=0.06$). C-peptide of insulin elevations were somewhat less dramatic, but more statistically significant (2.1-fold, $p<0.005$ versus pre-treatment values; 1.9-fold, $p<0.04$ versus NeoADT values), likely because the longer half-life of c-peptide in the blood reduces variability induced by random differences in food intake. These elevations of insulin and c-peptide in combination with the small increases in blood glucose are consistent with increased peripheral insulin resistance induced by treatment with IMC-A12.

Lastly, IGFBP-1 protein levels would be predicted to decrease in response to increasing levels of insulin secretion seen with IMC-A12 treatment (Gualberto, et al, 2009). This is due to negative feedback regulation of IGFBP-1 production in the liver by insulin. However, no decrease is seen upon IMC-A12 treatment in our samples. In fact, there is a non-significant increase in IGFBP-1 levels compared to pre-treatment values (2-fold, $p=0.14$) (Figure 25). Secondly, the baseline levels of IGFBP-1 were lower on average in patients on the A12 study compared to the NeoADT cohort, a relative difference which persisted and increased to a significant 0.37-fold ($p<0.02$) level by the end of study. It should also be noted that the inverse was true when baseline IGF-II levels were compared between the two studies (Figure 24), although in the case of IGF-II, little increase was seen in the NeoADT cohort during treatment, while there were significant increases with IMC-A12 treatment as discussed above. The IGFBP-1 changes are most consistent with IMC-A12-induced insulin insensitivity in the liver.

In sum, changes in serum insulin, c-peptide and glucose are all consistent with those effects predicted by effective IGF-1R blockade. The IGFBP-1 effects bear further examination, but the simplest explanation is that insulin sensitivity is reduced in the liver, preventing the expected IGFBP-1 decreases with IMC-A12 treatment-associated increased insulin levels. In a similar fashion, lack of proportionality between blood glucose changes and the insulin/c-peptide changes suggests the possibility of IMC-A12-induced peripheral insulin resistance resulting in substantially increased insulin levels need to achieve similar levels of blood glucose control. This is also consistent with IMC-A12-induced diabetes in two of the A12 patients, which was readily controlled with metformin, an insulin-sensitizer.

Correlations of serum biomarkers with clinical PSA outcomes: Discovery of biomarkers of response to IGF-1R inhibition

In general, PSA responses to the combination of IMC-A12 and hormonal therapy were excellent, with nadir PSA values at 0.1%-3.5% of initial values. Castrate testosterone levels were achieved in all patients. In absolute terms, nadir PSA values ranged from 0.02 to 2.5 (Median = 0.13) as depicted in Figure 26 In an initial exploratory analysis, A12 patients were stratified into 2 groups based on median nadir PSA- low PSA or better responders and high PSA or worse responders. For most of the biomarkers described above, no quantitative or statistically significant differences were seen, as illustrated by growth hormone levels (Figure 26). This has the interesting implication that PSA responses in these patients are not due to differences in A12 on-target efficacy. Alternatively, there may be subtle differences in anti-IGF-1R activity that these biomarkers are insensitive to, or differences between anti-IGF-1R effectiveness in the pituitary versus the prostate.

By contrast, in the case of insulin and c-peptide of insulin, PSA stratification revealed significant differences in the secreted levels of these factors in response to IMC-A12 treatment. Patients with better response to therapy (low PSA group) had very little increase in circulating insulin levels while on treatment, while the patients with lesser therapy responses (high PSA group) had substantial insulin increases, reaching levels 5.3-fold ($p<0.02$) higher than good responders (Figure 26). As expected, the c-peptide of insulin was also higher (2.1-fold, $p<0.002$) in the high PSA group, compared to patients with better PSA responses. Interestingly, despite the increased insulin and c-peptide levels, blood glucose levels also rose (non-significantly) in the patients with lesser responses to therapy, compared to the better responders (1.3-fold, $p=0.14$). By contrast, as observed above, there were no significant differences in the insulin-repressed IGFBP-1 levels seen in these two groups despite the significant differences in circulating insulin levels (Figure 26). The lack of IGFBP-1 level change differences further suggest that IMC-A12 confers central (liver) insulin resistance equally in all patients, in contrast to the differences in IMC-A12-induced peripheral insulin resistance.

Thus, the worse-responding patients appear to account for majority of IMC-A12-induced insulin resistance changes seen when cohort is analyzed as one group. These data intriguingly suggest that patients with greater A12-induced insulin insensitivity will have lesser responses to IGF-1R inhibition. If this is the case, then insulin changes in response to IGF-1R inhibitor therapy may allow prediction of response to such therapy. To our knowledge, this is the first reported biomarker of response to this class of agents. Of note, PSA responses did not correlate with IGF-I or IGF-II changes, altered levels of which have previously been correlated with or implicated in therapy resistance mechanisms (Garofalo et al, 2011; Gualberto et al, 2011). Thus, in the case of prostate cancer, the significance of these biomarkers is substantially less than that of the insulin/c-peptide changes.

Body mass index, clinical responses, and biomarker effects

Body mass index and other factors associated with the metabolic syndrome and insulin resistance have been repeatedly linked to prostate cancer development rates, aggressiveness of disease, and even survival (Albanes et al, 2009; Ma, et al, 2008). Above, we have clearly established that A12 treatment results in elevated levels of insulin without corresponding decreases in IGFBP-1, and out of proportion to blood glucose changes. This directly implies A12-induced peripheral and liver insulin resistance. Secondly, our exploratory analyses have shown that patients with better PSA responses to A12 treatment do not have the significant insulin/c-peptide

increases seen in patients with lesser PSA responses. To seek further understanding of this issue, the effects of pre-treatment body mass index (BMI) in this trial were evaluated.

The median pre-treatment BMI (29.7) in the A12 population was similar to that in the NeoADT cohort (BMI=28) (Table 2). Given the biomarker changes described above, it would be predicted that the lesser-responding patients (high PSA group) would have a higher BMI. In fact, when compared, pre-treatment BMI values averaged 28.1 for the low PSA group and 32.2 for the high PSA group ($p=0.10$) (Figure 9). Although non-significant, the trend is clear. Unfortunately, pre-treatment BMI could not predict for nadir PSA response ($p=0.70$, data not shown), thus pre-treatment BMI alone is not sufficient to predict response to A12.

Also as expected, the low BMI patients had lesser changes in insulin (0.25x, $p=0.06$) and c-peptide (0.78, $p=0.06$) (Figure 9) compared to the high BMI group in response to A12 treatment (although these were of borderline statistical significance). Most interestingly, both groups had a similar lack of IGFBP-1 decreases in response to insulin, but the pre-treatment levels were substantially different. The low BMI group had significantly higher baseline IGFBP-1 levels compared to the high BMI group (4.1x, $p<0.03$), consistent with less pre-treatment insulin resistance in the low BMI group (Figure 27).

A particularly interesting conclusion which can be drawn from this data is that there are inherent differences between pre-treatment, baseline insulin resistance as shown by differences in baseline IGFBP-1 levels which do not correlate with PSA response, and the insulin resistance which is induced on treatment with A12 and which does correlate with PSA response. This suggests possible biological differences between these processes and invites further investigation to characterize these differences.

Conclusions:

Serum biomarkers of the IGF pathway provide strong evidence supporting on-target efficacy of A12 combined with ADT, both compared to pre-treatment controls, and compared to an ADT-only control cohort. Serum biomarkers also suggest peripheral insulin resistance and novel evidence of liver insulin resistance. Exploratory analyses comparing patients with PSA nadir responses above versus below the median find no differences in the biomarkers of on-target efficacy. Despite this, a novel correlation has been discovered suggesting induction of insulin resistance by A12 is linked with with worse responses to the therapy (higher nadir PSA values). Pre-treatment BMI tends to be higher in the patients who respond less well to A12, but pre-treatment BMI can not predict for PSA response. Given a significant correlation of A12-induced insulin resistance with PSA response, the lack of PSA response correlation with pre-treatment IGFBP-1 levels strongly suggests differences between pre-treatment and A12-induced insulin resistance states. Finally, the strong correlation of pre-treatment IGFBP-1 with pre-treatment BMI - and the lack of correlation with PSA response - may provide insight into the limitations of BMI as a pre-treatment A12 predictive biomarker.

Objective 3b: *Design and execute a clinical trial combining docetaxel chemotherapy with an inhibitor of senescence-associated modulation of cancer cell survival in the neoadjuvant setting prior to radical prostatectomy. The anti-IGF1R antibodies such as IMC-A12 (Imclone) or CP-751,871 (Pfizer) are currently the lead candidates for inhibition. Other candidates/pathways will be considered and optimized during the clinical trial design phase of the project in year 3.*

Task 31. Write the protocol and required regulatory documents. (Months 24-30)

This trial was not fully developed for several reasons. First, it was deemed clinically infeasible due to drug/company and ethical considerations. Second, it would have directly conflicted with the resources and patients during the the timeline required to complete the neoadjuvant trial of IMC-A12 combined with androgen deprivation.

Task 32. Obtain regulatory approval from Institutional Review Board. (Months 30-34)

As per Task 31.

Task 33. Develop recruitment materials, hold in-service for clinical providers and study coordinator. (Months 34-36)

As per Task 31.

Task 34. Recruit, enroll, and treat patients on study. Monitor and report adverse events. (Months 36-60)

As per Task 31.

Task 35. Analyze pre- and post-treatment tissues for changes senescent cell content and senescence-associated signaling molecule expression as described above (Objectives 1a. and 1c.). (Months 40-55)

As per Task 31.

Task 36. Collate and analyze data. (Months 34-60)

As per Task 31.

Technical Objective 4: To complete data analyses, compile accomplishments and reportable outcomes, and write final project reports and manuscripts.

Objective 4a*: Prepare manuscript 1.*

Task 37. Describe changes in the extent and distribution of senescent cells in the prostate as a function of chemotherapy and androgen ablation therapies. Correlate with alterations in senescence-associated signaling molecules, gene expression studies and clinical outcome measures. (Months 38-44)

A manuscript characterizing the regulation of STC1 secretion levels in response to various environmental conditions. Parts of these data were presented at the AACR Annual Meeting, 2007. STC1-specific data were presented at the PCRP IMPACT meeting, March 2011.

Several iterations of this manuscript have been prepared, with the lastest submitted to my mentor Dr. Peter Nelson at the end of January 2011. It has been Dr. Nelson's opinion that the described results were not of a desired impact level for publication and manuscripts have not been submitted for consideration at any journals.

Objective 4b: *Prepare manuscript 2.*

Task 38. Describe the effects of docetaxel, mitoxantrone, and IMC-A12 treatment on the nude mouse model of senescence-dependent carcinogenesis and progression. Inter-correlations of presence or absence of tumor, size of grafts, extent and distribution of senescent cells and levels of senescence-associated signaling molecules. (Months 24-30)

As per Task 17.

Objective 4c: *Prepare manuscript 3.*

Task 39. Describe the clinical efficacy, side effect profile, and laboratory correlates data resulting from the combination of IMC-A12 with androgen ablation. (Months 50-60)

The above data was presented in large part at the Genitourinary Cancers Symposium, February 2011. A manuscript has been prepared and circulated among co-authors. After initial review, it was decided that inclusion of laboratory analyses on the balance of the treated patients would significantly strengthen the manuscript. These analyses are ongoing. On completion, I anticipate submission of a revised manuscript with the complete data set.

Subsequent planned manuscripts stemming from this trial and laboratory analyses will include characterization of the clinical pathological effects of this treatment, tissue immunohistochemistry to directly evaluate the effects of this treatment on various proteins (including but not limited to senescence-associated-β-galactosidase, androgen receptor, IGF-1R, signaling molecules downstream of IGF-1R, etc.), and gene expression analyses from both an unbiased global perspective as well as analyses focused on androgen responsive genes, a gene signature developed in prostate cancer xenografts treated with A12, and others of interest. I will be the primary author or a major co-author on all these manuscripts.

Objective 4d: *Prepare manuscript 4.*

Task 40. Describe the clinical efficacy, side effect profile and laboratory correlate study results from the clinical trial combining IMC-A12 with chemotherapy. (Months 54-60)

As per Task 31.

Key Research Accomplishments

• We employed the Senescence-Associated-β-Galactosidase histochemical stain to investigate the effects of chemotherapy on induction of senescence in the cells of the prostate. Staining was adequate to identify epithelial cells in which senescence has taken place. Senescence could not be identified in the stromal compartment of the prostate. Despite an optimized assay, it was clear that senescence changes identified by this method occur too infrequently to allow statistically significant correlations with changes when compared to pre-treatment tissues.

• We established the staining conditions for the senescent cell markers p16(INK4a) and DcR2. We have validated these methods using a unique tissue microarray of aging and prostate cancer. For both of these biomarkers of senescence, we have demonstrated statistically significant increases in benign epithelial cell senescence and in stromal senescence that correlate with aging. We have also demonstrated statistically significant increases in neoplastic epithelial staining by these markers when compared to benign epithelial staining, irrespective of patient age.

Localization of STC1 in human prostate tissue compartments by immunohistochemistry- Cancer and benign, young and old, naïve or after hormonal and chemotherapy treatment

• We established the staining conditions for the secreted senescence-associated proteins STC1, GDF15, CXCL1, IL8, IGF-1R. Never before examined in the human prostate, we have demonstrated significant association of increased STC1 staining in neoplastic epithelium, compared to benign epithelium. In addition, there is weak (and not statistically significant) association of increased STC1 staining in the stroma that occurs with aging and an even more weak association

of decreased STC1 staining that occurs with aging in the benign epithelium. We have also demonstrated a significant increase in GDF15 staining in the neoplastic prostate epithelium, compared to benign epithelium.

• Based on staining conditions optimized using the TMA of aging as described in the last report, we stained a series of the post-chemotherapy-treated patient samples for STC1. To allow comparison with pre-treatment tissues, these were frozen, rather than FFPE samples. Unfortunately, despite further optimization for this type of sample, levels of background staining were seen which significantly limit our ability to interpret these results. There do appear to be staining of stroma, benign epithelium and neoplastic epithelium, but staining differences with and without antibody are a matter of slight changes in intensity.

• To better understand STC1 staining in the prostate and motivated by its intriguing and limited data in other organs and unknown role in the prostate, we performed an experiment staining serial prostate sections for various markers likely to be found in the stroma, including fibroblasts/myofibroblasts, dendritic cells, endothelium, macrophages, and neuronal cells. We have demonstrated co-localization of STC1-staining cells with the neuronal markers S100 and Neurofilament. We have also demonstrated co-localization of STC1 with the fibroblastic/myofibroblastic markers Caldesmon and Sm-a-actin. The neuronal staining appears to be uniform, suggesting high levels of STC1 expression irrespective of age or treatment status. By contrast, only a small fraction of the fibroblastic compartment stains for STC1, suggesting this may be a marker for altered or abnormal cells. Alternatively, STC1 may define a novel subset of the fibroblastic stroma of unknown signficance.

<u>Characterization of Stanniocalcin 1 (STC1) secretion modulators in the environment, and the consequences of these changes on cellular function</u>

• STC1 secretion from prostate stromal cells was found to be induced by calcium, phosphate, osmotic stress, and hypoxic conditions. Strength of osmotic stress and concentration of calcium and phosphate were all associated with increased STC1 secretion in a concentration-dependent fashion.

• Increasing serum concentrations mediated increased STC1 secretion from the prostate stromal cells. One or more heat-labile factors account for a small portion of the STC1 secretion effect, but most of the effect is heat-insensitive.

• Most, but not all, forms of senescence induction result in senescent prostate stromal cells which have increased levels of STC1 secretion. These include oxidative stress (hydrogen peroxide), DNA damage (bleomycin), replicative exhaustion (telomere shortening), and Ras oncogene-induced (Ras overexpression), but not p16 overexpression.

• The MAPK signaling pathway appears to play the largest role in mediating increased STC1 secretion in response to environmental conditions, but the PKA and PI3K pathways also contribute.

• STC1 secretion from prostate stromal cells was found to be significantly increased by the c-met inhibitor SU11274 in a dose-dependent fashion, but there is no significant effect of HGF treatment.

• Prior to establishment of the senescent cellular state, STC1 secretion is increased by ongoing chemotherapy treatments with docetaxel and bleomycin, but not mitoxantrone in the prostate stromal cell lines.

• In addition to the prostate stromal cell lines, PC3 cells, but not primary epithelial cell lines or LNCaP cells are found to secrete dectectable (albeit significantly lower than the prostate stromal lines) levels of STC1. STC1 secretion from PC3 cells is induced by similar, although not identical conditions as with the prostate stroma.

• No substantial and consistent changes were seen in the docetaxel sensitivity or resistance of various epithelial prostate cell lines upon modulation of STC1 effects by addition of purified STC1 protein or anti-STC1 antibody treatment.

• Correlative work has demonstrated treatment-associated gene expression changes in senescence cell markers and senescence-associated proteins. These are consistent with proteomics data we presented at the 2007 AACR Annual Meeting, April 14-18, 2007. There are many chemotherapy treatment-related gene expression changes in the benign epithelium, neoplastic epithelium, and the stromal compartments consistent with senescence changes, as determined by quantitative real-time PCR on samples obtained by laser-capture microscopy.

• We secured essential funding for the clinical trial proposed in Technical Objective 3a. I acquired clinical trials design and implementation training at the ASCO/AACR Methods in Clinical Cancer Research workshop, July 28-August 3, 2007. Significantly ahead of the proposed timeline, we have completed final revisions to the protocol, obtained Investigational New Drug application approval from the Food and Drug Administration and approval of the protocol by the Fred Hutchinson/University of Washington Center Cancer Consortium Scientific Review Committee. Final review by the University of Washington Human Subjects Review Committee V is ongoing. Regulatory paperwork for U.S. Army Medical Research and Materiel Command's Office of Research Protections, Human Research Protection Office review is in preparation and will be submitted shortly.

• Modulation of STC1 levels by addition of recombinant purified STC1 and by addition of anti-STC1 polyclonal antibodies were found to not affect proliferation of LNCaP, Du145 or PC3 cells, alone, or with ATP, with or without serum.

• STC1 modulation also did not significantly alter LNCaP, Du145 or PC3 cell proliferation/survival when grown under hypoxic conditions.

• Chemotherapy responses of BPH1, LNCaP, Du145 or PC3 cells to docetaxel or mitoxantrone were not affected by modulation of STC1 levels.

• BPH1, Du145 and PC3 cellular motility in a wound healing assay were not altered by STC1 modulation in the presence or absence of ATP.

• Although I demonstrated substantial and consistent upregulation of steroidogenic enzymes in the castration-resistant cell lines Du145 and PC3 compared to the androgen-dependent cell line LNCaP, there were no significant alterations evident after modulation of STC1 levels.

<u>A neoadjuvant clinical trial of IMC-A12 plus ADT: Initial laboratory analyses of the first 18 consecutive patients and correlation with clinical outcomes</u>

• The desired high risk population was accrued to the clinical trial and the treatment has been well-tolerated, but the clinical benefits have been minimal. Last patient completed treatment in June, 2011.

• Laser capture microdissection of the stromal, benign epithelial, and cancerous epithelial compartments has begun from both pre-treatment biopsy tissue, as well as post-treatment prostatectomy tissue.

• Serum biomarkers interrogating alterations in homeostasis of the IGF pathway are consistent with on-target efficacy of this combined treatment. Stratification of the patients based on nadir PSA suggests that the PSA differences are not due to differences in IMC-A12 on-target efficacy.

• The biomarkers of the glucose-insulin homeostatic pathway are consistent with A12-induced peripheral, as well as liver insulin resistance. Even more interestingly, the bulk of elevations of insulin and c-peptide occur largely in the patients who have higher nadir PSA levels. Thus, higher levels of peripheral insulin resistance induced by A12 are correlated with the clinical PSA outcome in response to A12 treatment. In addition to being one of the first biomarkers of response to IGF-1R inhibitors, this also is suggestive of possible mechanisms of resistance to these inhibitors.

• As predicted, body mass index in the PSA response groups correlated with the insulin resistance of each respective group. Unfortunately, pre-treatment BMI could not predict for PSA outcome.

• Although there was very little difference in IGFBP-1 levels between the PSA outcome groups, stratification by BMI identified significant differences in baseline IGFBP-1 levels, consistent with the predicted differences in average circulating insulin levels due to higher peripheral insulin resistance in higher BMI patients.

• The differences between baseline peripheral insulin resistance and A12-induced peripheral and liver insulin resistances, as well as the different patterns of resistance seen when stratifying by PSA compared to BMI would indicate that additional factors likely play a role in overall response to IGF-1R inhibitors.

Reportable Outcomes

Publication:
Dean JP, Higano CS. Does Chemotherapy Have a Role Before Hormone-Resistant Disease Develops? Current Urology Reports, 10(3)226-35. 2009.

Dean, JP, Nelson, PS. Profiling influences of senescent and aged fibroblasts on prostate carcinogenesis. Br J Cancer; 2008 Jan 29:98(2):245-249.

Abstracts:
Wright JL, **Dean JP**, Lin DW, Dalkin B, Ellis WJ, Corman J, Mostaghel E, Nelson P, Wan J, Haugk K, Cohen P, Ludwig D, Montgomery B, Plymate S. Neoadjuvant insulin-like growth factor receptor 1 (IGF-1R) blockade with androgen deprivation in men with prostate cancer undergoing radical prostatectomy. Northwest Urological Society 58th Annual Scientific Conference, Portland, OR. December 2011.

Lee F, Harris WP, Yu EY, Shenoi J, Champion T, **Dean JP**, Gore JP, Porter MP, Wright JL. Pathologic response rates from neoadjuvant chemotherapy in muscle invasive urothelial carcinoma of the bladder. Northwest Urological Society 58th Annual Scientific Conference, Portland, OR. December 2011.

Dean JP, Coleman I, Sun Y, Martin D, Nelson P. Identification and Characterization of STC1 as a Paracrine Senescence Factor in the Prostate Tumor Microenvironment. Innovative Minds in Prostate Cancer Today (IMPaCT) Conference, Orlando, FL. March 2011.

Dean JP, Montgomery B, Wan J, Cohen P, Haugk K, Corman JM, Ellis WJ, Dalkin BL, Ludwig DL, Plymate SR. On-target activity of neoadjuvant cixutumumab and combined androgen deprivation therapy for high-risk prostate cancer, a phase II trial.
2011 Genitourinary Cancers Symposium, Orlando, FL. February 2011.

Plymate, S, Cohen, P, **Dean J**, Lin, D, Ludwig, DL, Montgomery, RB. Serum markers of response in a neo-adjuvant clinical trial of the IGF-IR mabA12 in prostate cancer. Fifth International Congress of the GRS and the IGF Society, New York, NY. October 2010.

Dean JP, Plymate SR, Dalkin BL, Ellis WJ, Lin DW, Wright, JW, Corman, JM, Lange PH, True, LD, Montgomery, B. Neoadjuvant IMC-A12 and combined androgen deprivation with prostatectomy for high risk prostate cancer, a phase II trial, Clinical Trials in Progress, ASCO Annual Meeting, June 2010.

Dean JP, Coleman I, Martin DB, Nelson, PS. Potential mediators of prostate carcinogenesis identified through quantitative analysis of the extracellular proteome associated with prostate fibroblast senescence [abstract]. In: Proceedings of the 98th Annual Meeting of the American Association for Cancer Research; 2007 Apr 14-18; Los Angeles, CA. Philadelphia (PA): AACR; 2007. Abstract nr 2788.

Chapter:
Montgomery RB, **Dean J**, Plymate S. 2010. The role of Insulin-like Growth Factor signaling in prostate cancer development and progression, Smith J (ed) IGFR in Cancer. Springer, NY, NY. 2011 (in press).

Conclusions

The research accomplished in this proposal has provided valuable insight regarding senescence and senescence-related factors and their association with and importance in prostate cancer biology and treatment. Within the limits of an optimized Senescence-Associated β-Galactosidase assay, we have demonstrated that senescent cells do not appear to accumulate upon treatment with chemotherapy. On the other hand, quantitative real-time PCR quantitation of gene expression changes support the likelihood of chemotherapy-induced accumulation of senescence changes. We have established the immunohistochemical conditions for staining prostate tissues for the senescent cell markers p16 and DcR2. Using a Tissue Microarray of Aging and Prostate Cancer, we have validated these staining protocols and demonstrated a correlation between chronological aging and increased staining of these proteins in benign epithelium and the prostate stroma.

We have used a similar approach to establish staining conditions for the senenescence-associated, secreted proteins GDF15, STC1, CXCL1, and IL8. Although optimized staining results of CXCL1 and IL8 were disappointing, there GDF15 and STC1 staining were interpretable. Of these, STC1 has been further investigated in detail as a novel biomarker of senescence and its potential contribution to prostate cancer, metastasis and response to treatment. We showed that STC1 was expressed at significantly higher levels in the benign epithelium, compared to the neoplastic epithelium. There was also an increase in stromal STC1 staining with aging which approached statistical significance. Further work examined STC1 staining of post-chemotherapy-treated tissues. Staining was identified in the benign, neoplastic and stromal compartments. Unfortunately, unexpected background staining in the negative controls limits our ability to interpret these results, particularly given the limited numbers of cases and amounts of tissue available for analysis. Under these limitations, it may not be possible to achieve statistical significance. We also examined STC1 staining of bony metastases from heavily pre-treated patients. In these patients, STC1 shows staining similar to that seen in untreated primary prostate tissues. Lack of changes in STC1 with metastasis and treatment may imply a lack of influence on these processes, or may simply reflect an ongoing process that is not affected by the change in microenvironment.

STC1 localization in the stromal compartment has been more fully characterized with a serial section co-immunostaining approach. We have demonstrated uniform staining of neuronal cell bundles and individual neuronal cells in the prostate stroma. STC1 was also found localized to a small fraction of fibroblastic/myofibroblastic cells. Thus, STC1 staining may represent a fraction of these cells which have undergone senescence changes, may represent a previously undefined compartment in the fibroblastic stroma, or both.

STC1 was further established as a response biomarker of senescence and microenvironmental stressors, both in the stromal and in the epithelial compartment. Changes in STC1 secretion

were seen in response to increased serum, inhibition of c-met signaling, increased calcium and phosphate, osmotic stress, hypoxia, induction of senescence, and ongoing treatment with chemotherapy. The MAPK signaling pathway appears to be of primary importance in the STC1 secretion increases with stress, but the PKA and PI3K pathways also contribute. Together, these data suggest a model whereby STC1 secretion is a generalized response to stressful microenvironmental conditions.

An in vivo role for STC1 is strongly implied by changes in STC1 gene expression after neoadjuvant chemotherapy treatment. The consequences of this are suggested by changes in chemotherapy resistance upon modulation of STC1 activity in cell culture models.

The possible functional consequences of increased STC1 in the prostate microenvironment in response to the broad variety of stressful conditions were tested. Unfortunately, neither increased STC1 nor decreased STC1 were found to cause significant changes in proliferation, survival under hypoxic conditions, response or sensitivity to chemotherapy, cell motility/wound healing, or modulation of intracrine androgen metabolism.

At the conclusion of the funding period, the neoadjuvant clinical trial of IMC-A12 with androgen deprivation had completed accrual and treatment has concluded. The monoclonal antibody IMC-A12 blocks signaling through the IGF-1R protein, previously established as an important signaling pathway in prostate cancer and proposed as an important pathway in senescence based on my preliminary data.

Initial studies of serum biomarkers from the first consecutive 18 patients have revealed good evidence for on-target efficacy and treatment-induced peripheral and liver insulin resistance. Stratification of patients into response groups based on nadir PSA suggests response may not be due to lack of IMC-A12 on-target efficacy, but due to differences in treatment-induced peripheral insulin resistance. Pre-treatment body mass index was found to be correlated with PSA response but not sufficient to predict for PSA response. By contrast, pre-treatment BMI did correlate very well with baseline differences in insulin resistance- much more so than PSA response. Therefore although pre-treatment BMI likely contributes, there are additional factors which significantly contribute to response to this combination therapy.

Work required to facilitate tissue gene expression analyses was more than half-completed. Specifically, frozen blocks of pre-treatment core biopsies and post-treatment prostatectomy blocks had been sectioned and laser capture microscopy performed to capture populations of stroma, benign epithelium and neoplastic epithelium. These frozen sections will also be suitable for the senescence-associated b-d-galactosidase histochemistry. Further planned work by a post-doc funded by the parent study will result in purification, amplification and gene analyses by quantitative real-time PCR as well as microarray hybridization to gain quantitation on a global scale, as well as exacting quantitation of selected genes of interest (including the genes previously found to be altered in the senescent state).

Together, these studies continue to define novel aspects of the prostate microenvironment and how senescence-associated factors may play an important role in prostate tumor biology and response to therapies.

References

Bavik C, Coleman I, Dean JP, Knudsen B, Plymate S, and Nelson, PS, Cancer Research, 2006, 66(2)794-802.

Knudsen BS and Edlund M, Advances in Cancer Research, 2004, 91:31-67.

Zlot C, Ingle G, Hongo J, Yang S, Sheng Z, Schwall R, Paoni N, Wang F, Peale FV and Gerrisen ME, 2003, The Journal of Biological Chemistry, 278(48)47654-47659.

Albanes D, Weinstein SJ, Wright ME, Männistö S, Limburg PJ, Snyder K, Virtamo J. Serum insulin, glucose, indices of insulin resistance, and risk of prostate cancer. J Natl Cancer Inst. 2009 Sep 16;101(18):1272-9.

Bavik C, Coleman I, Dean JP, Knudsen B, Plymate S, Nelson PS. The gene expression program of prostate fibroblast senescence modulates neoplastic epithelial cell proliferation through paracrine mechanisms. Cancer Res. 2006 Jan 15;66(2):794-802.

Block GJ, DiMattia GD, Prockop DJ. Stanniocalcin-1 regulates extracellular ATP-induced calcium waves in human epithelial cancer cells by stimulating ATP release from bystander cells. PLoS One. 2010 Apr 20;5(4):e10237.

Coppé JP, Patil CK, Rodier F, Sun Y, Muñoz DP, Goldstein J, Nelson PS, Desprez PY, Campisi J. Senescence-associated secretory phenotypes reveal cell-nonautonomous functions of oncogenic RAS and the p53 tumor suppressor. PLoS Biol. 2008 Dec 2;6(12):2853-68.

Gualberto A, Pollak M. Emerging role of insulin-like growth factor receptor inhibitors in oncology: early clinical trial results and future directions. Oncogene. 2009 Aug 27;28(34):3009-21.

Gualberto A, Hixon ML, Karp DD, Li D, Green S, Dolled-Filhart M, Paz-Ares LG, Novello S, Blakely J, Langer CJ, Pollak MN. Pre-treatment levels of circulating free IGF-1 identify NSCLC patients who derive clinical benefit from figitumumab. Br J Cancer. 2011 Jan 4;104(1):68-74.

Garofalo C, Manara MC, Nicoletti G, Marino MT, Lollini PL, Astolfi A, Pandini G, López-Guerrero JA, Schaefer KL, Belfiore A, Picci P, Scotlandi K. Efficacy of and resistance to anti-IGF-1R therapies in Ewing's sarcoma is dependent on insulin receptor signaling. Oncogene. 2011 Jan 31. [Epub ahead of print]

Huang F, Hurlburt W, Greer A, Reeves KA, Hillerman S, Chang H, Fargnoli J, Graf Finckenstein F, Gottardis MM, Carboni JM. Differential mechanisms of acquired resistance to insulin-like growth factor-i receptor antibody therapy or to a small-molecule inhibitor, BMS-754807, in a human rhabdomyosarcoma model. Cancer Res. 2010 Sep 15;70(18):7221-31.

Luo CW, Kawamura K, Klein C, Hsueh AJ. Paracrine regulation of ovarian granulosa cell differentiation by stanniocalcin (STC) 1: mediation through specific STC1 receptors. Mol Endocrinol. 2004 Aug;18(8):2085-96.

Ma J, Li H, Giovannucci E, Mucci L, Qiu W, Nguyen PL, Gaziano JM, Pollak M, Stampfer MJ. Prediagnostic body-mass index, plasma C-peptide concentration, and prostate cancer-specific mortality in men with prostate cancer: a long-term survival analysis. Lancet Oncol. 2008 Nov;9(11):1039-47.

Montgomery RB, Mostaghel EA, Vessella R, Hess DL, Kalhorn TF, Higano CS, True LD, Nelson PS. Maintenance of intratumoral androgens in metastatic prostate cancer: a mechanism for castration-resistant tumor growth. Cancer Res. 2008 Jun 1;68(11):4447-54.

Titus MA, Schell MJ, Lih FB, Tomer KB, Mohler JL. Testosterone and dihydrotestosterone tissue levels in recurrent prostate cancer. Clin Cancer Res. 2005 Jul 1;11(13):4653-7.

Ulanet DB, Ludwig DL, Kahn CR, Hanahan D. Insulin receptor functionally enhances multistage tumor progression and conveys intrinsic resistance to IGF-1R targeted therapy. Proc Natl Acad Sci U S A. 2010 Jun 15;107(24):10791-8.

Untergasser G, Koch HB, Menssen A, Hermeking H. Characterization of epithelial senescence by serial analysis of gene expression: identification of genes potentially involved in prostate cancer. Cancer Res. 2002 Nov 1;62(21):6255-62.

Appendices

none

Supporting Data

TABLE 1. Senescence biomarkers on a Tissue Microarray of Aging and Prostate Cancer

Optimized protocols for immunohistochemistry of the indicated molecule were used to stain a tissue microarray of aging, comprised of cores from young men (aged <50) or old (aged >70) with prostate cancer diagnosis. The cores were selected to include both benign epithelium and neoplastic epithelium. Stained sections were scored with a board-certified, GU cancer specialist pathologist, noting the intensity (0, 1+ or 2+) and extent (expressed in % cells) of each of the three compartments: Benign epithelium, cancer epithelium and stroma. Staining scores of each compartment in each core were pooled into comparative groups to evaluate with 2-sample, 2-tailed T-tests for significance of the differences in staining and expressed as the average and standard deviation of the staining score for each compartment.

FIGURE 1. STC1 staining of prostate tissues from the TMA of aging.

Representative examples of the STC1 immunohistochemistry staining of the tissue microarray of aging and prostate cancer are depicted. Arrows denote: 1, Gleason pattern 3 glands; 2, 1+ and diffuse glandular staining; 3, 2+ and focal glandular staining; 4, diffuse stromal staining; 5, nerve bundles; 6, nerves or myofibroblasts.

FIGURE 2. STC1 staining of post-chemotherapy tissue KP-02.

STC1 staining as with Figures 1 and 2 was performed on the flash-frozen, post-chemotherapy treatment tissues from patient KP-02. Negative control composed of pre-immune serum instead of primary antibody is also shown.

FIGURE 3. STC1 staining of post-chemotherapy tissue KP-03.

STC1 staining as with Figures 1 and 2 was performed on the flash-frozen, post-chemotherapy treatment tissues from patient KP-03. Negative control composed of pre-immune serum instead of primary antibody is also shown.

FIGURE 4. STC1 staining of post-Chemo-Hormonally treated Bone Metastases.

Representative images were obtained from a tissue microarray comprised of tissue cores obtained from patients who underwent rapid autopsy. STC1 staining was as in Figures 1 and 2.

FIGURE 5. Serial Section staining of STC1 and Caldesmon.

Consecutive serial sections obtained from a single neoplastic prostate gland were stained for STC1 as in Figures 1 and 2, as well as the standard pathological marker Caldesmon. The STC1-stained sections flank the Caldesmon-stained section.

FIGURE 6. Serial Section staining of STC1 and Sm-a-actin.

Consecutive serial sections obtained from a single neoplastic prostate gland were stained for STC1 as in Figures 1 and 2, as well as the standard pathological marker Sm-a-actin. The STC1-stained sections flank the Sm-a-actin-stained section.

FIGURE 7. Serial Section staining of STC1 and Neurofilament.

Consecutive serial sections obtained from a single neoplastic prostate gland were stained for STC1 as in Figures 1 and 2, as well as the standard pathological marker Neurofilament. The STC1-stained sections flank the Neurofilament-stained section.

FIGURE 8. Serial Section staining of STC1 and S100.

Consecutive serial sections obtained from a single neoplastic prostate gland were stained for STC1 as in Figures 1 and 2, as well as the standard pathological marker S100. The STC1-stained sections flank the S100-stained section.

FIGURE 9. Changes in gene expression levels with chemotherapy treatment

Quantitative real-time PCR was performed to quantitate gene expression levels for the various listed proteins. Templates were comprised of diluted cDNA derived from laser-captured cells from each of the listed tissue compartments after purification and amplification. Threshold cycles were normalized to the "housekeeping" gene RPL13a. Two sample, two-tailed T-tests were used to compare the pre- and post-chemotherapy gene expression levels with significance expressed as p-values.

FIGURE 10. STC1 gene expression in the human prostate before and after neoadjuvant chemotherapy treatment

STC1 gene expression was quantitated using quantitative real-time PCR, normalized to RPL13a, after laser capture microscopy, RNA isolation, amplification, and reverse transcription. 2-sample, 2-tailed T-test was used to calculate p-values.

FIGURE 11. STC1 secretion in response to hypoxia- additive effects of serum and osmotic stress.

Equal numbers of prostate stromal cells were treated with the indicated additives for 3 days under hypoxic or normoxic conditions, then conditioned medium was collected and equal quantities probed for STC1 by Western Blot.

FIGURE 12. STC1 secretion in response to calcium, phosphate and osmotic stress.

Equal numbers of prostate stromal cells were treated with the indicated additives for 3 days, then conditioned medium collected and equal quantities probed for STC1 by Western Blot.

FIGURE 13. STC1 secretion in response to varied concentrations of native and boiled fetal bovine serum.

Equal numbers of prostate stromal cells were treated with the indicated serum concentration for 3 days, then conditioned medium collected and equal quantities probed for STC1 by Western Blot.

FIGURE 14. STC1 secretion from senescent prostate stromal cells: Various modes of senescence induction.

Equal quantities of medium conditioned by prostate stromal cells made senescent by each of the displayed methods (ASB- Bleomycin, ASH- Hydrogen Peroxide, RS- replicative exhaustion, pRAS- Ras oncogene overexpression, p16- p16 overexpression, pDEST- control vector) were collected and equal quantities probed for STC1 by Western Blot.

FIGURE 15. STC1 secretion after treatment with cell signaling inhibitors.

Equal numbers of prostate stromal cells were treated with the indicated agents for 3 days, then conditioned medium collected and equal quantities probed for STC1 by Western Blot.

FIGURE 16. STC1 secretion in response to HGF and the c-met inhibitor SU11274.

Equal numbers of prostate stromal cells were treated with the indicated agents for 3 days, then conditioned medium was collected and equal quantities probed for STC1 by Western Blot.

FIGURE 17. STC1 secretion from prostate stromal cells undergoing chemotherapy treatments.

Equal numbers of prostate stromal cells were treated with the indicated agents for 3 days, then conditioned medium collected and equal quantities probed for STC1 by Western Blot.

FIGURE 18. STC1 secretion from PC3 cells, response to environmental conditions.

Equal numbers of prostate PC3 cells were treated with the indicated agents under the indicated conditions for 3 days, then conditioned medium collected and equal quantities probed for STC1 by Western Blot.

FIGURE 19. Effects of STC1 modulation on cell proliferation. Equal numbers of the indicated cell line were plated into 96 well plates, treated with the indicated treatment for 3 days, then MTS assay used to quantitate relative cell numbers. Data represent averages of quadruplicate wells and standard deviation.

FIGURE 20. Effects of STC1 modulation on growth in Hypoxia. Equal numbers of the indicated cell line were plated into 96 well plates, treated with the indicated treatment and incubated under hypoxic (1% Oxygen) conditions with MTS assay used to quantitate relative cell numbers across 6 days. Data represent averages of quadruplicate wells and standard deviation.

FIGURE 21. Effects of STC1 modulation on chemotherapy response. Equal numbers of the indicated cell line were plated into 96 well plates, treated with the indicated STC1-modulating treatment overnight, then docetaxel or mitoxantrone at the indicated concentrations (nM) were added. MTS assay was used to quantitate relative cell numbers after 3 days of treatment. Data represent averages of quadruplicate wells and standard deviation.

FIGURE 22. Effects of STC1 modulation on cell migration. Indicated cell lines were grown to 90%+ confluency then a sterile pipet tip was used to denude a central region. After careful rinsing, growth media containing the indicated treatment was added to the plate. Marked locations were serially photographed at the indicated times and migration of the cell fronts into the denuded area was measured on photographic prints. Data represent averages of quadruplicate wells and standard deviation.

FIGURE 23. Expression of androgen metabolic genes by PC3 and LNCaP cell lines. After isolation and reverse transcription of RNA from the indicated cell lines, relative quantities of the indicated enzymes were quantitated by real-time PCR. Once normalized to RPL13a, levels from the PC3 cell line were compared with the LNCaP expression levels. Red “up” arrows denote enzymes with increased message in PC3 relative to LNCaP and green “down” arrows indicated decreased message in PC3 relative to LNCaP.

TABLE 2. Study patient characteristics. Clinical characteristics of the initial consecutive 18 patients on the neoadjuvant study of IMC-A12 with androgen deprivation are listed. This is the cohort from whom serum biomarkers were assayed and are described in this manuscript. In addition, the clinical characteristics of a control study of neoadjuvant androgen deprivation therapy-only are shown. These characteristics are stratified into clinically relevant groups and the median is described.

TABLE 3. Clinical pathological and Adverse event outcomes. The clinical pathological effects of the neoadjuvant IMC-A12 treatment regimen are listed and compared to predications made by the Kattan pre-operative clinical nomogram. The adverse events noted in patients on the neoadjuvant IMC-A12 clinical trial are listed, categorized by severity (Grade) and ascribed relatedness.

FIGURE 24. Effects of IGF-1R blockade and hormone therapy on IGF pathway homeostasis. ELISA assays were used to quantitate the indicated protein factor from serum obtained prior to treatment (Entry) or at the time of IMC-A12 infusion # 1, 3 or 5 (A12 #1, A12 #3, A12 #5) and at the time of prostatectomy (RRP). Patient samples are from the IMC-A12 study (A12) are shown in blue and neoadjuvant hormonal therapy only (NeoADT). Each data point represents the average value with SEM errors. Fold-change is calculated as A12 average divided by NeoADT average. Statistical 2-sample, 2-tailed t-tests are applied to compare the values indicated by asterisks to determine p-values.

FIGURE 25. Effects of IGF-1R blockade and hormone therapy on glucose homeostasis and insulin activity. ELISA assays were used to quantitate the insulin, c-peptide of insulin and IGFBP-1 levels from serum obtained prior to treatment (Entry) or at the time of IMC-A12 infusion # 1, 3 or 5 (A12 #1, A12 #3, A12 #5) and at the time of prostatectomy (RRP). Blood glucose at these time points was determined by clinical laboratory testing. Patient samples are from the IMC-A12 study (A12) are shown in blue and neoadjuvant hormonal therapy only (NeoADT). Each data point represents the average value with SEM errors. Fold-change is calculated as A12 average divided by NeoADT average. Statistical 2-sample, 2-tailed t-tests are applied to compare the values indicated by asterisks to determine p-values.

FIGURE 26. PSA responses and exploratory biomarker correlations. Nadir PSA- the lowest PSA achieved on the clinical trial- for each patient were plotted in waterfall plot. Nadir (0.13) is indicated by the arrow. The A12 patient cohort was stratified into low PSA (better responders-blue lines) and high PSA (worse responders- red lines). The average and SEM values for the indicated biomarkers were measured as described in Figures 6 and 7 for the two groups. Fold-change is calculated as “low PSA” group average divided by “high PSA” group average. Statistical 2-sample, 2-tailed t-tests are applied to compare the values indicated by asterisks to determine p-values for these differences.

FIGURE 27. Body Mass Index effects on clinical outcome and biomarkers. Pre-treatment body mass index (BMI) for patients on the IMC-A12 study were calculated and displays in this waterfall plot. Using the PSA stratification shown in Figure 8, the pre-treatment BMI values for patients in the two PSA response groups were compared. Average is shown as a line with individual values in a scatter fashion. Statistical 2-sample, 2-tailed t-tests are applied to determine p-values for the two groups. Patients were stratified based on pre-treatment BMI and the serum biomarker results for patients in the low and high BMI groups were calculated to determine average and SEM values. Fold-change is calculated as “low BMI” group average divided by “high BMI” group average. Statistical 2-sample, 2-tailed t-tests are applied to compare the values indicated by the asterisks to determine p-values for these differences.

TABLE 1. Senescence Biomarkers on a Tissue Microarry of Aging and Prostate Cancer

A. p16

Tissue Compartment	Staining Score Young Cohort	Staining Score Aged Cohort	2-sample 2-tailed t-test Young vs. Aged
Benign Epithelium	0.95 +/- 2.37	3.21 +/- 8.00	p<0.05
Neoplastic Epithelium	35.9 +/- 39.2	32.7 +/- 32.9	p=0.68
Stroma	0.92 +/- 1.60	2.16 +/- 5.38	p<0.05
2-sample, 2-tailed t-test Benign vs. Cancer	p<0.0001	p<0.0001	

B. DcR2

Tissue Compartment	Staining Score Young Cohort	Staining Score Aged Cohort	2-sample 2-tailed t-test Young vs. Aged
Benign Epithelium	16.5 +/- 22.2	39.1 +/- 32.9	p<0.0001
Neoplastic Epithelium	97.2 +/- 53.7	88.0 +/- 51.1	p=0.43
Stroma	0.19 +/- 0.82	0.70 +/- 2.22	p<0.05
2-sample, 2-tailed t-test Benign vs. Cancer	p<0.0001	p<0.0001	

C. STC1

Tissue Compartment	Staining Score Young Cohort	Staining Score Aged Cohort	2-sample 2-tailed t-test Young vs. Aged
Benign Epithelium	58.3 +/- 46.9	58.0 +/- 46.2	p=0.97
Neoplastic Epithelium	87.8 +/- 57.9	73.8 +/- 46.9	p=0.26
Stroma	57.2 +/- 36.8	67.0 +/- 40.0	p=0.09
2-sample, 2-tailed t-test Benign vs. Cancer	p<0.005	p=0.096	

D. GDF15

Tissue Compartment	Staining Score Young Cohort	Staining Score Aged Cohort	2-sample 2-tailed t-test Young vs. Aged
Benign Epithelium	99.6 +/- 68.1	87.9 +/- 54.2	p=0.23
Neoplastic Epithelium	165.7 +/- 45.0	158.9 +/- 42.3	p=0.48
Stroma	n.s.	n.s.	n.a.
2-sample, 2-tailed t-test Benign vs. Cancer	p<0.0001	p<0.0001	

Figure 1.

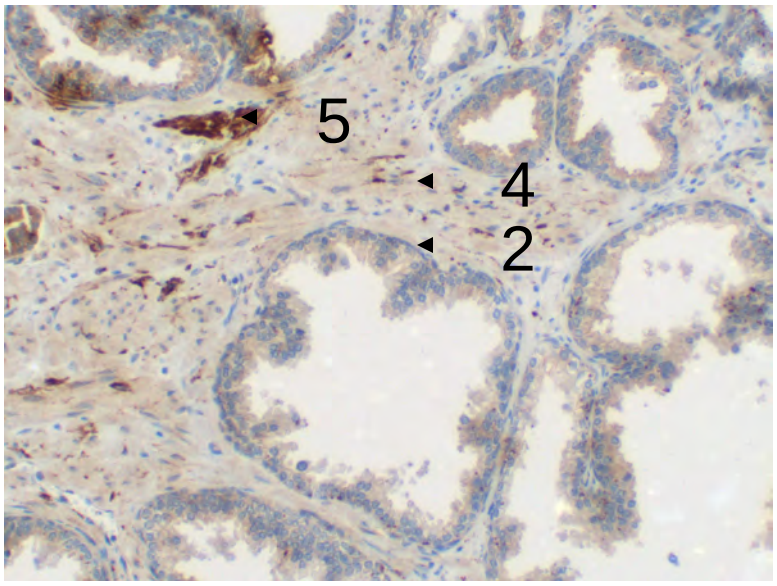

Benign Epithelium and Stroma

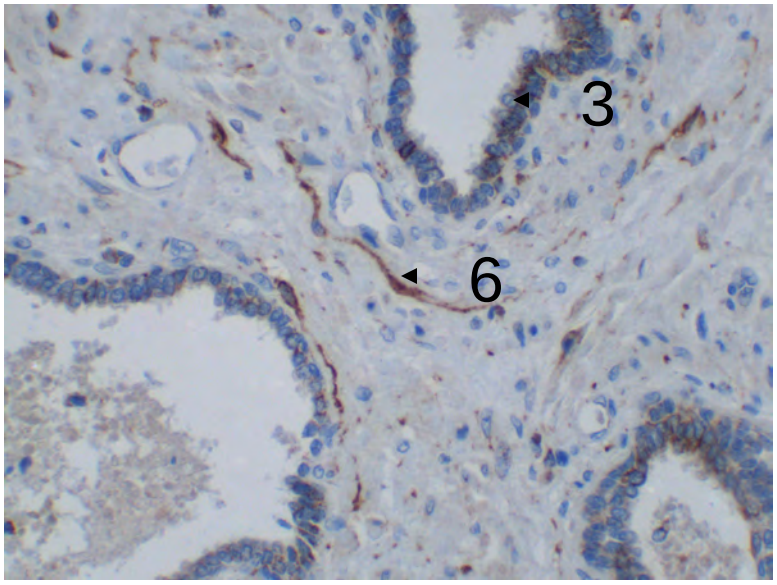

Benign Epithelium and Stroma

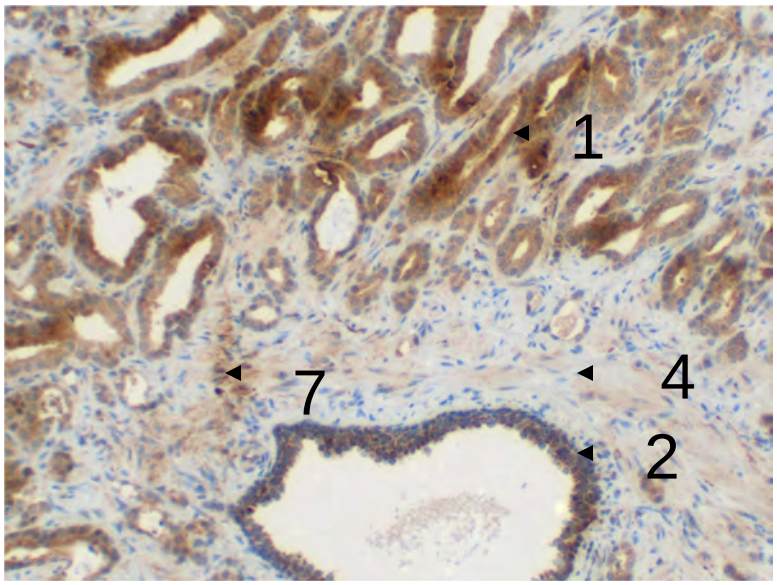

Gleason Pattern 3, Benign Epithelium And Stroma

Figure 2.

A

STC1

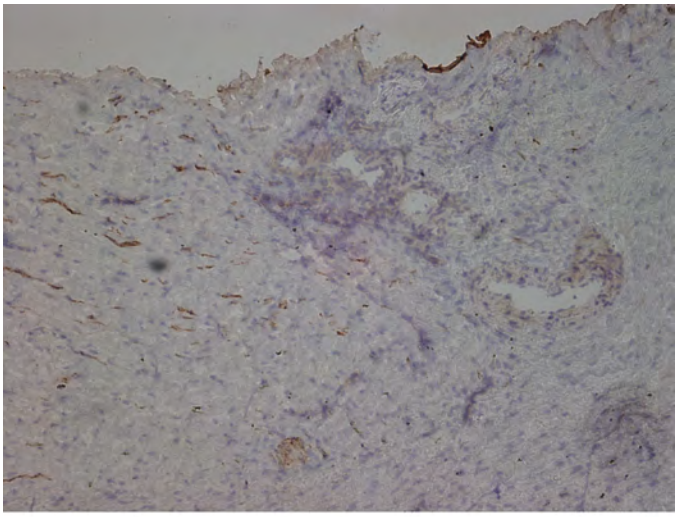

Negative control

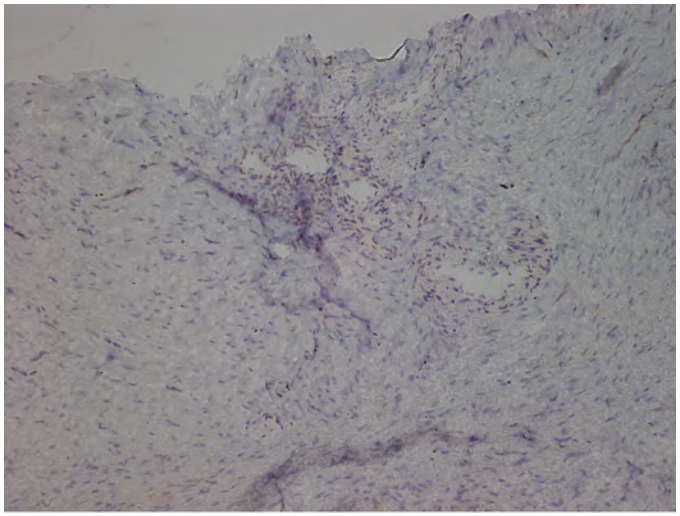

B

STC1

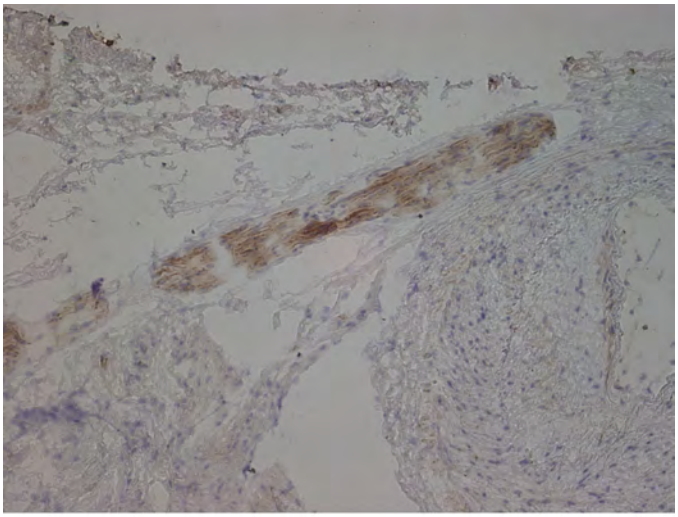

Negative control

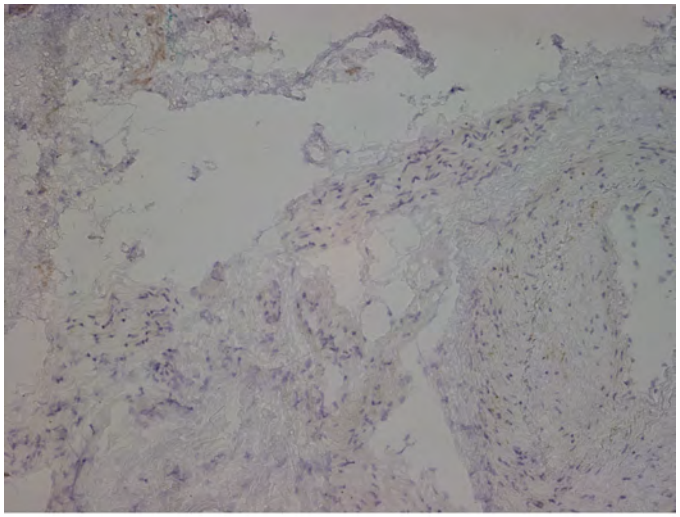

KP-02

Figure 3.

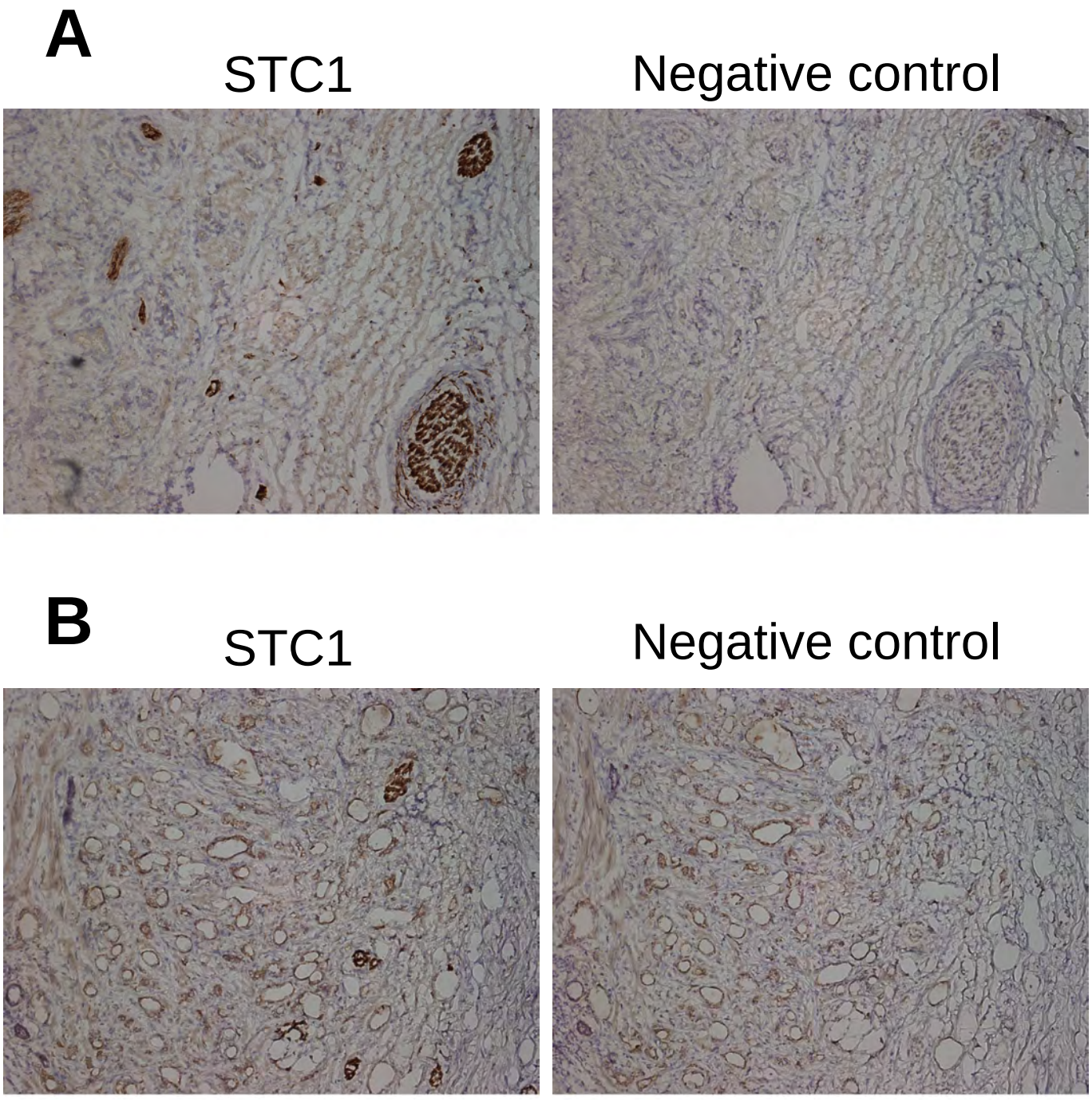

KP-03

Figure 4.

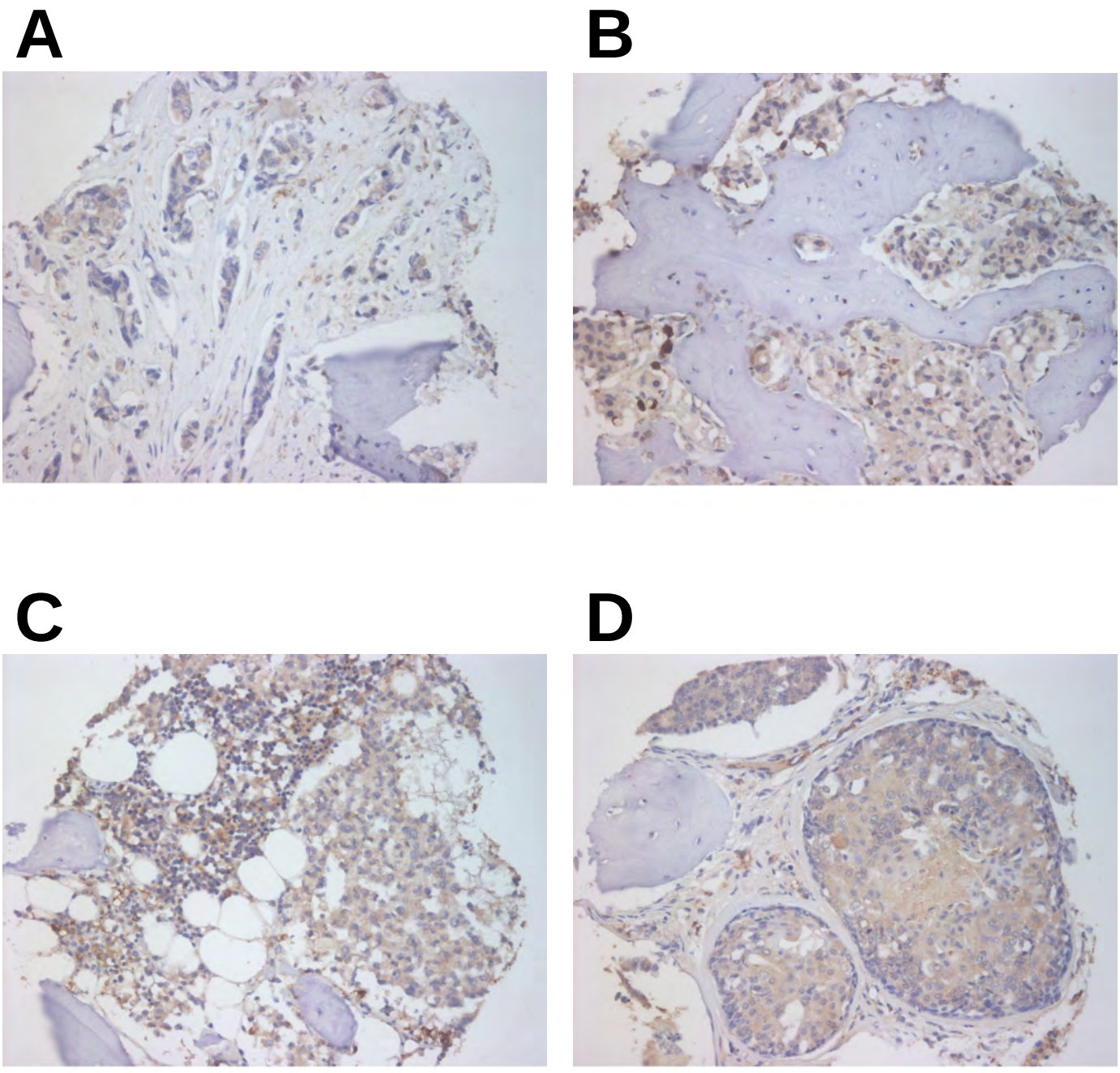

Figure 5.

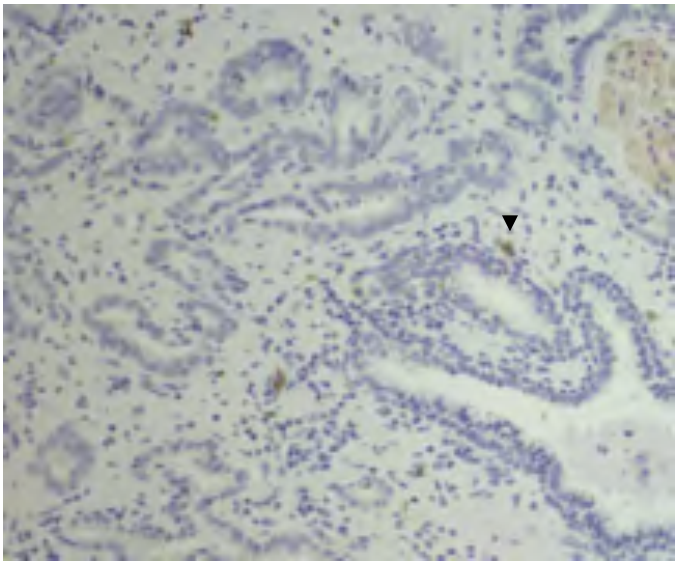

STC1

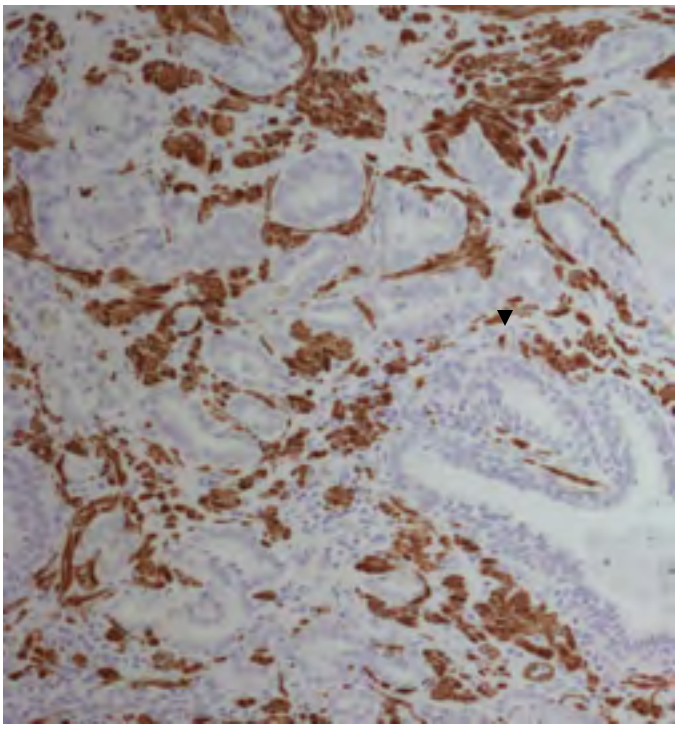

Caldesmon

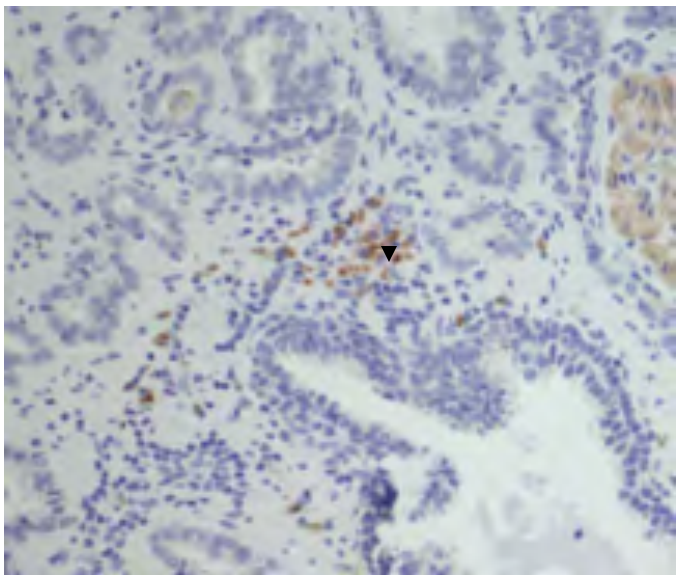

STC1

Figure 6.

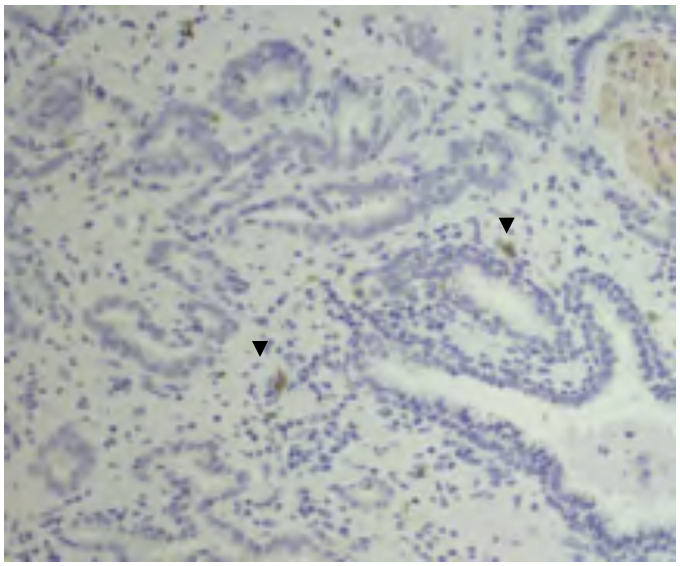

STC1

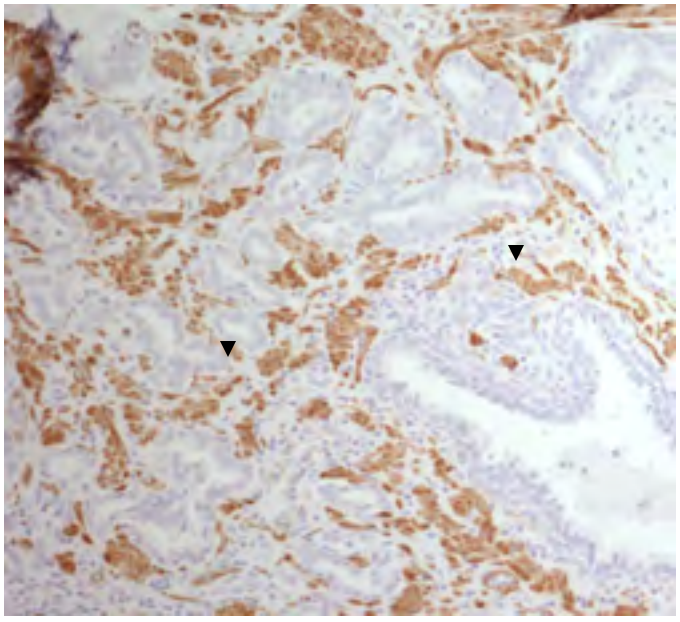

Sm-α-actin

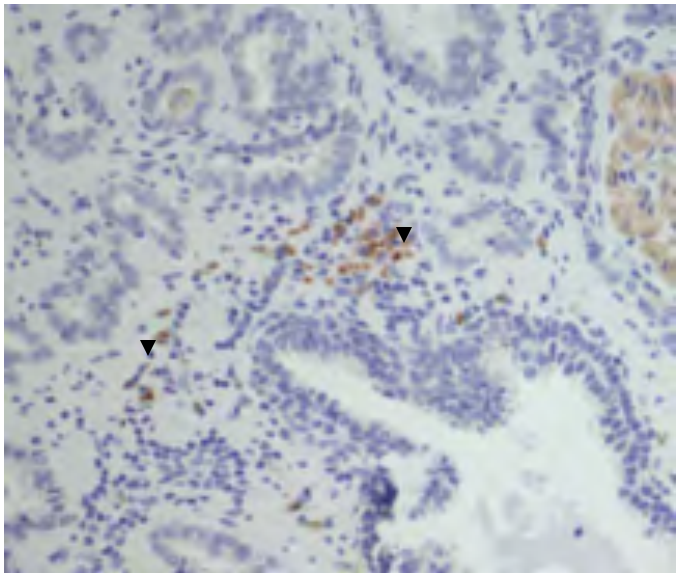

STC1

Figure 7.

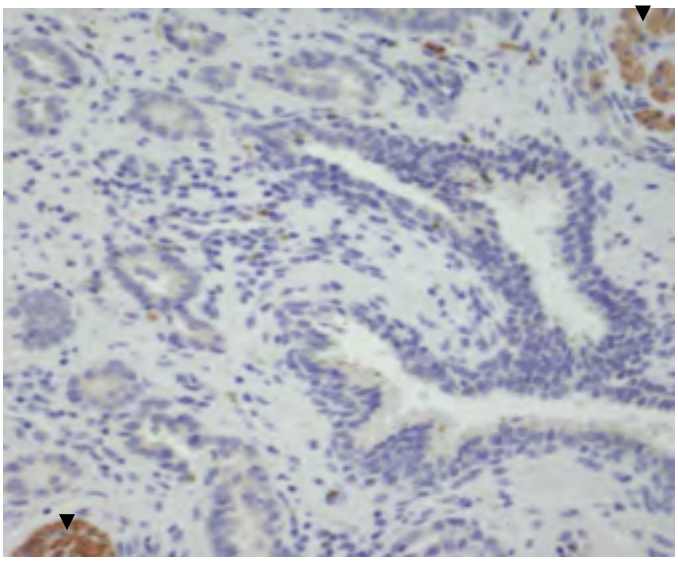

STC1

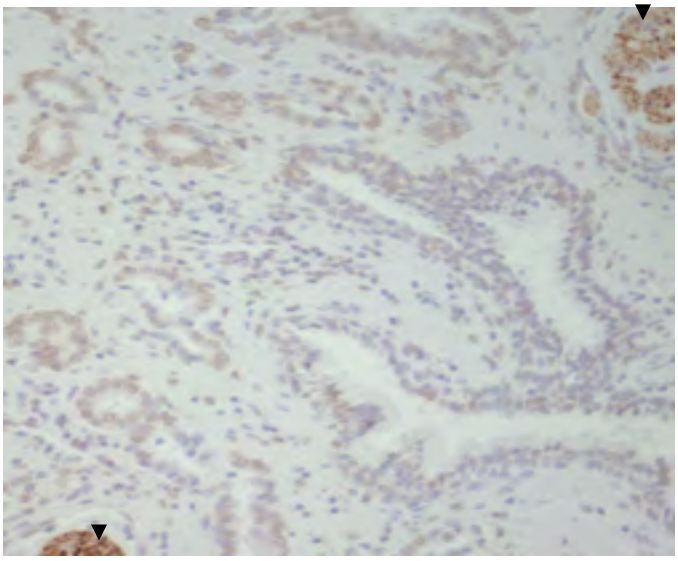

Neurofilament

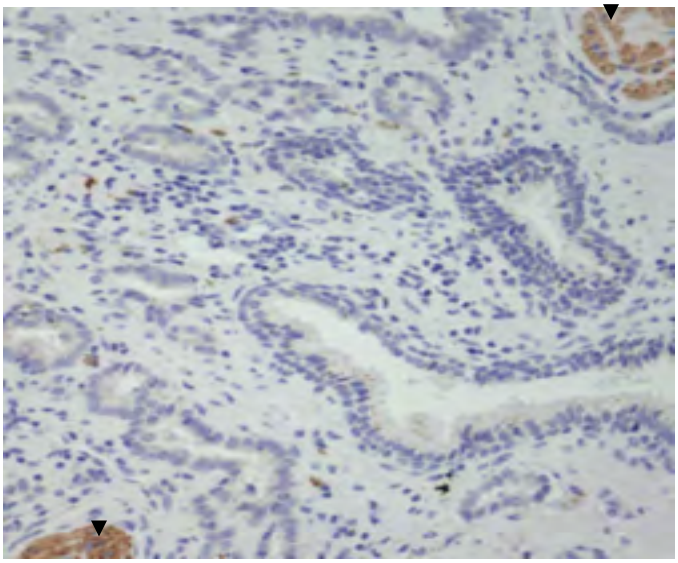

STC1

Figure 8.

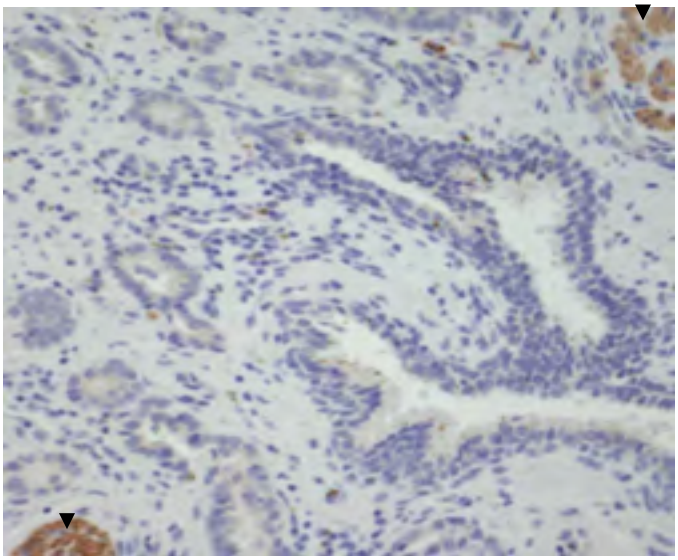

STC1

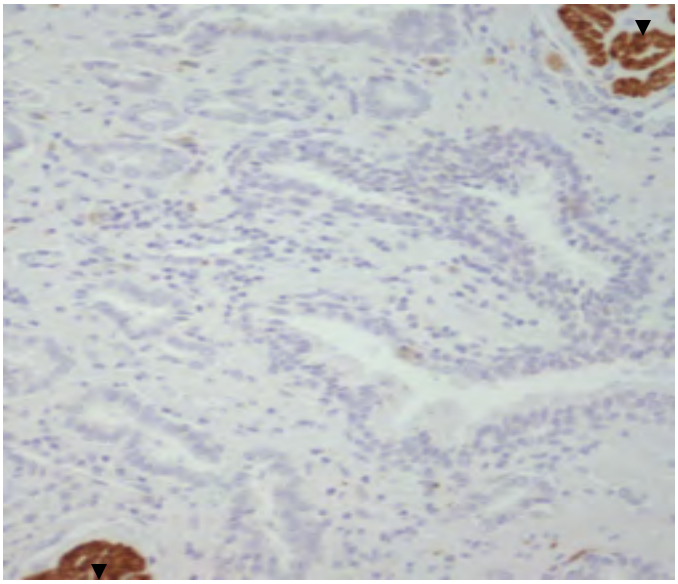

S100

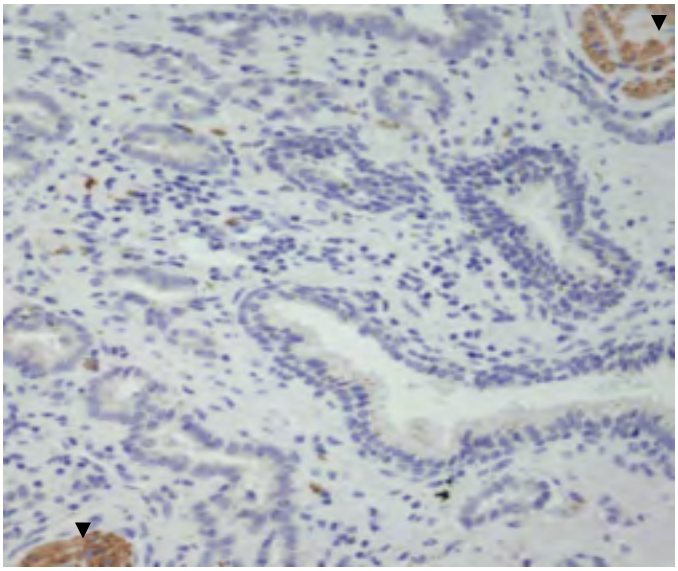

STC1

FIGURE 9. Changes in gene expression levels with chemotherapy treatment

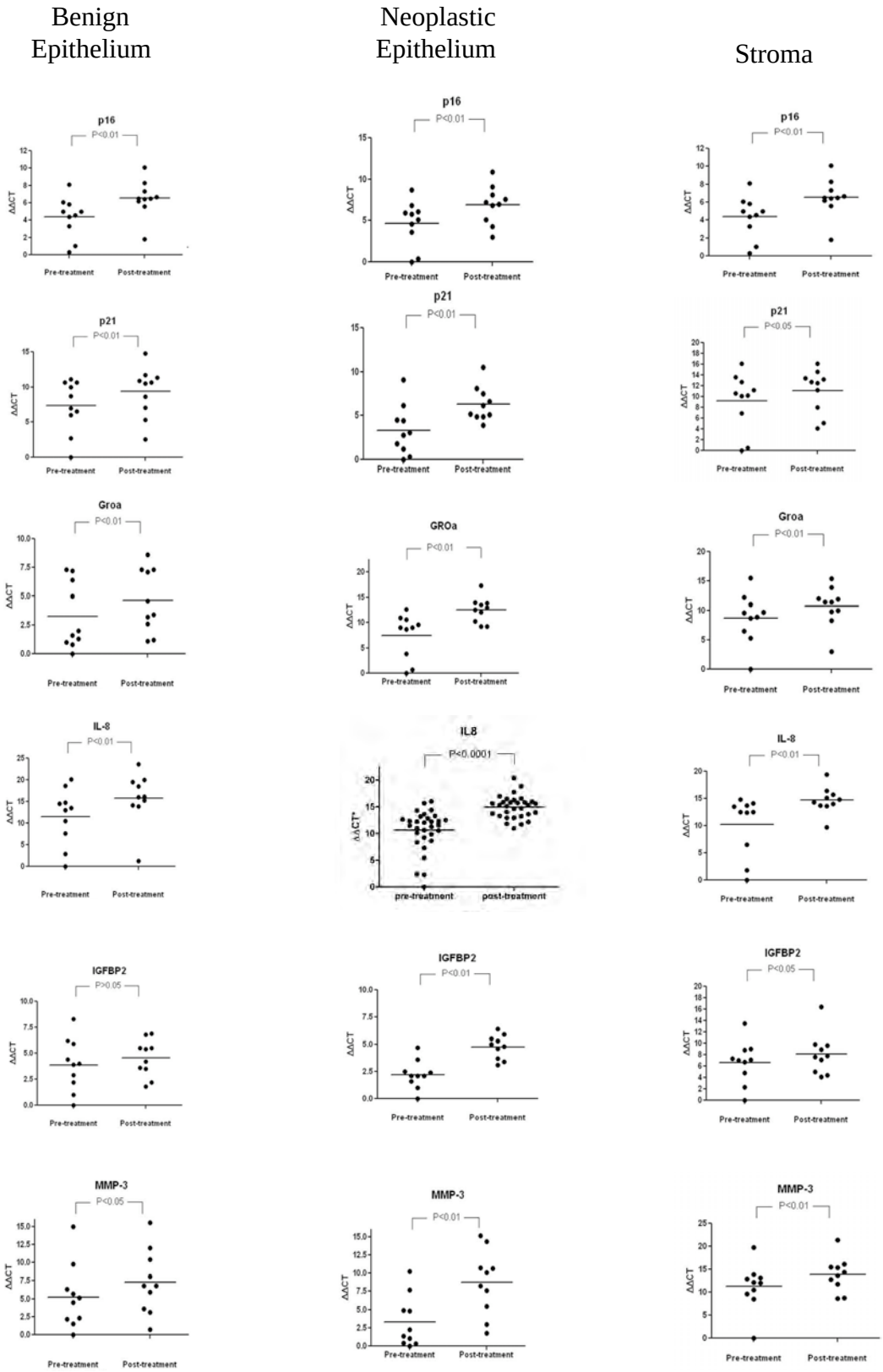

Figure 10

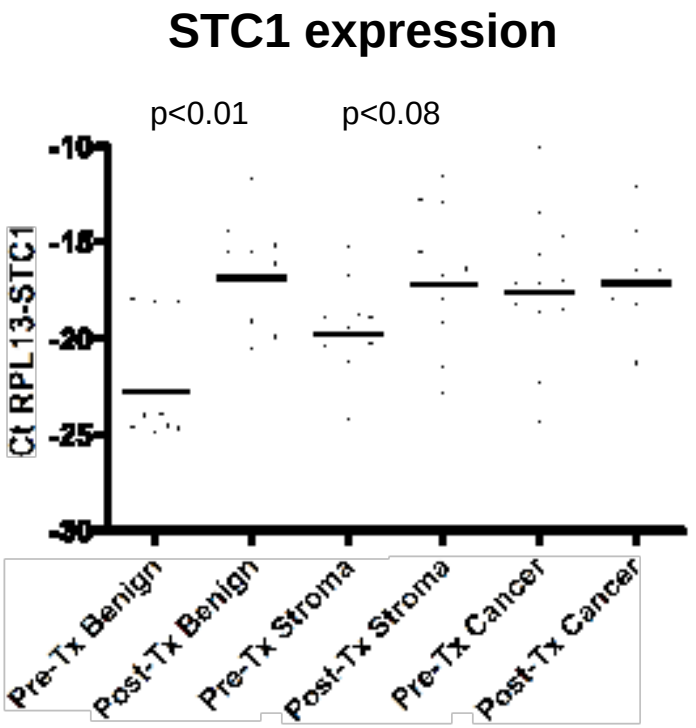
STC1 expression
p<0.01
p<0.08
Ct RPL13-STC1
-10
-15
-20
-25
-30
Pre-Tx Benign
Post-Tx Benign
Pre-Tx Stroma
Post-Tx Stroma
Pre-Tx Cancer
Post-Tx Cancer

Figure 11

A.

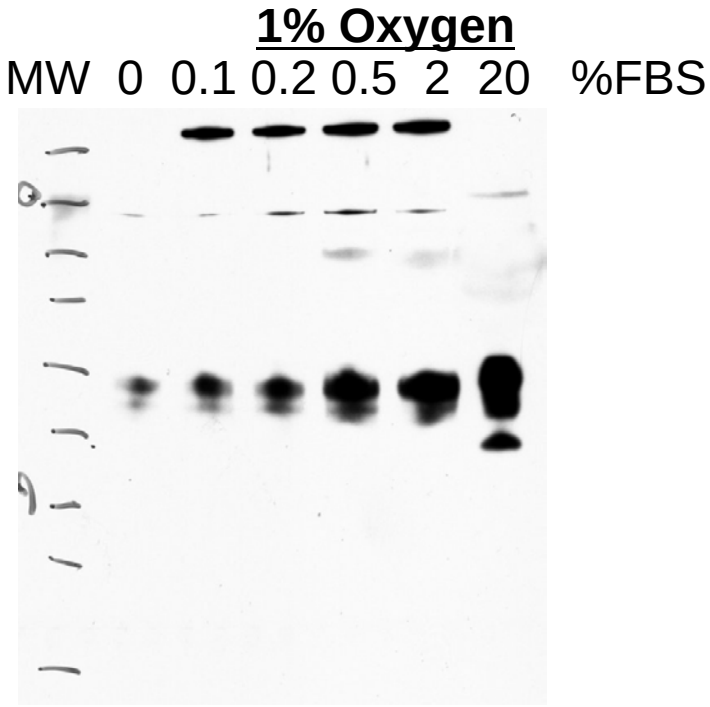
1% Oxygen
MW 0 0.1 0.2 0.5 2 20 %FBS

B.

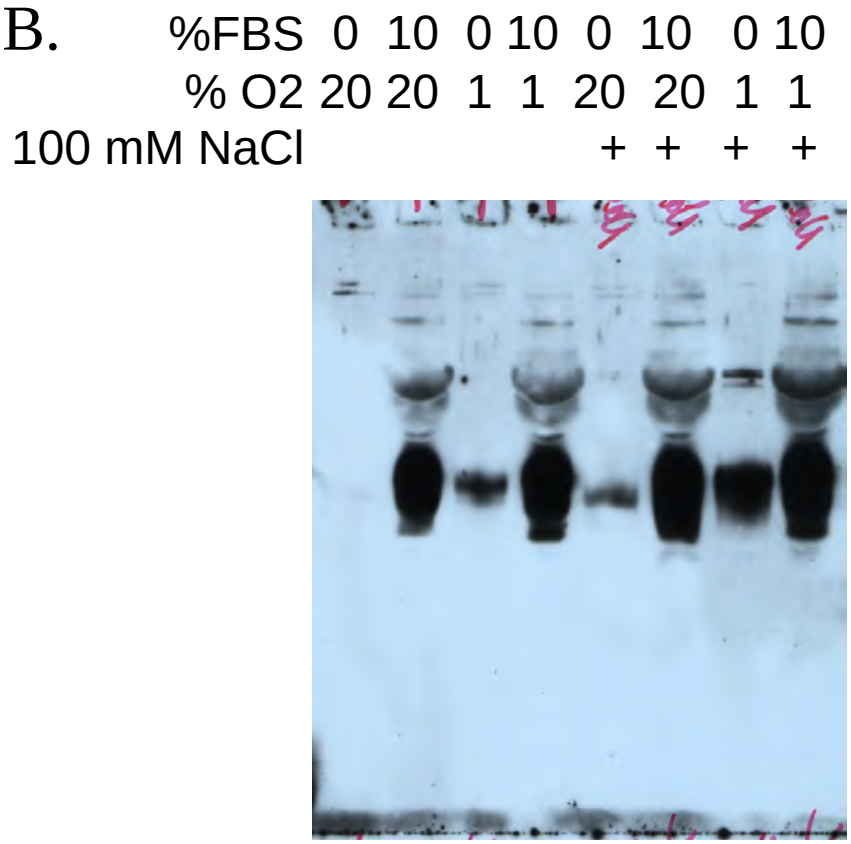
%FBS 0 10 0 10 0 10 0 10
% O2 20 20 1 1 20 20 1 1
100 mM NaCl + + + +

Figure 12

A.

mM CaCl2 0 1 5 20 100

mM MgCl2 1 5 20 0

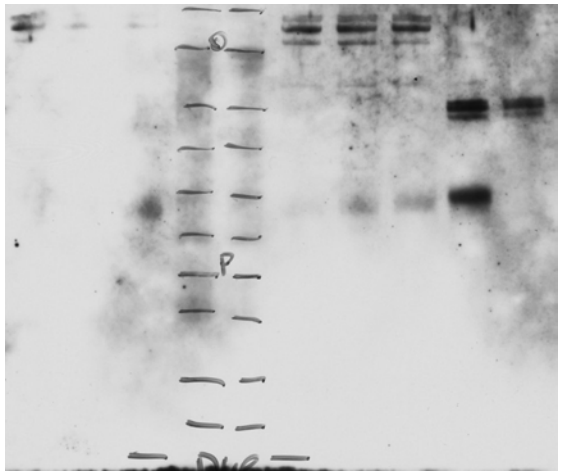

B.

mM NaPhosphate 0 1 5 10 50

mM NaSulfate 0 1 5 10

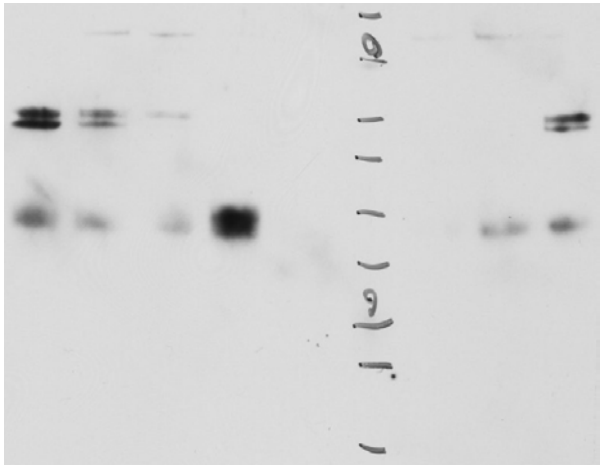

C.

Serum-Free

mM NaCl 0 50 100 200

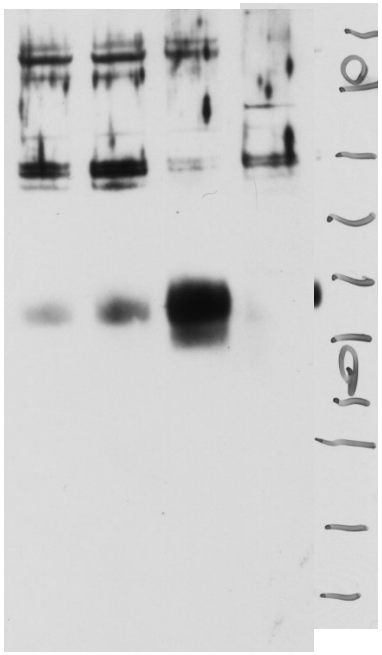

Serum-Containing

mM NaCl 0 50 100 200

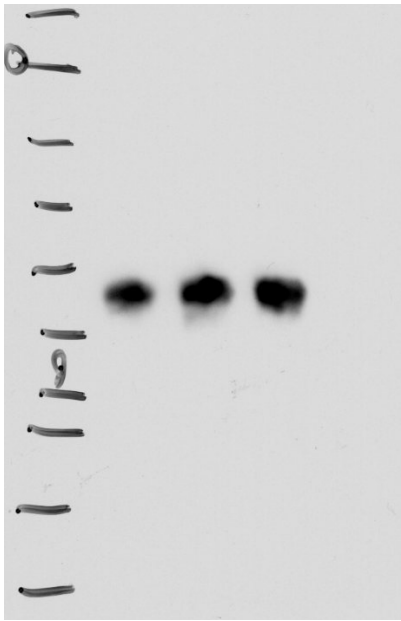

Figure 13

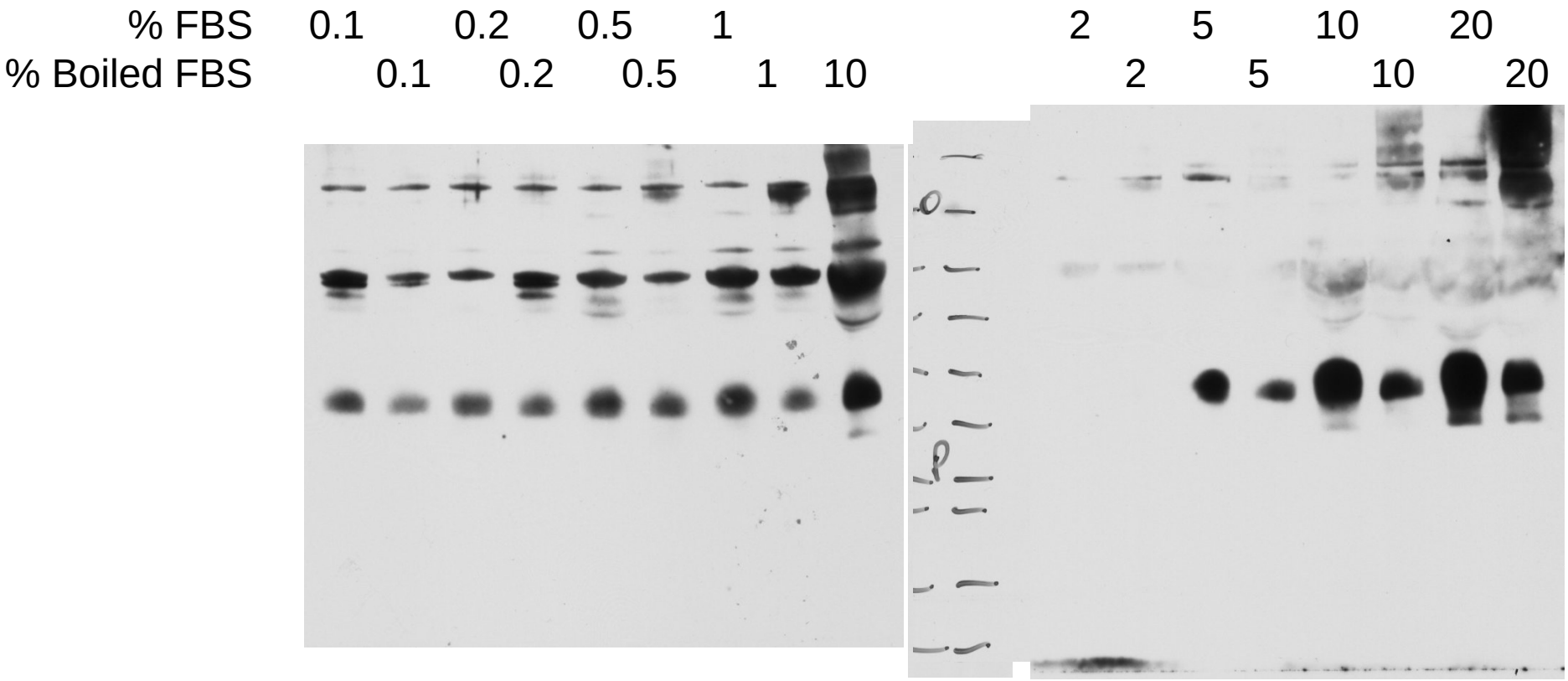

Figure 14

A.

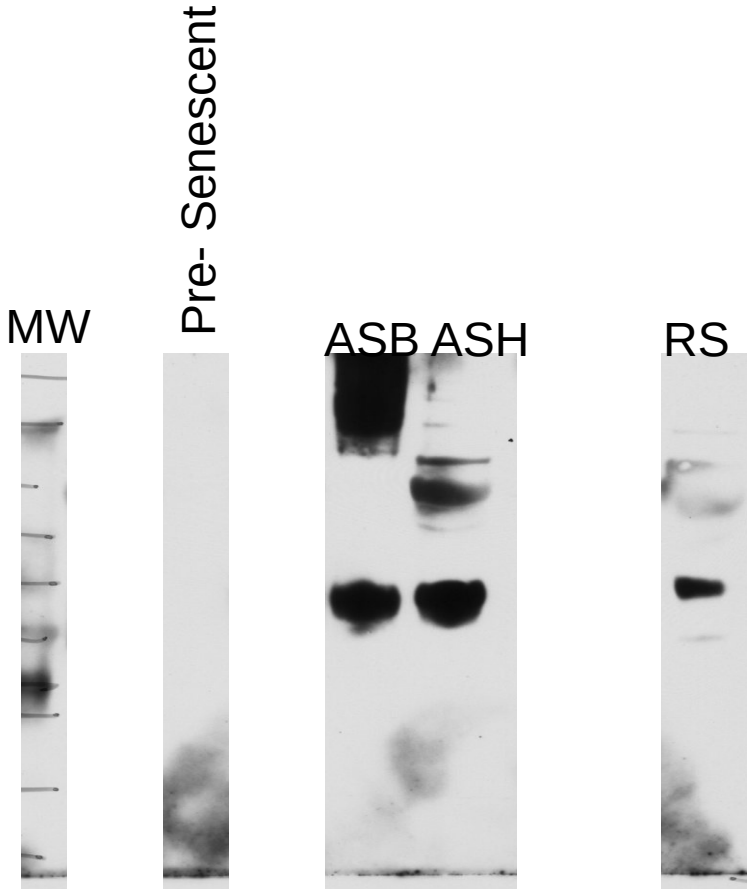

B.

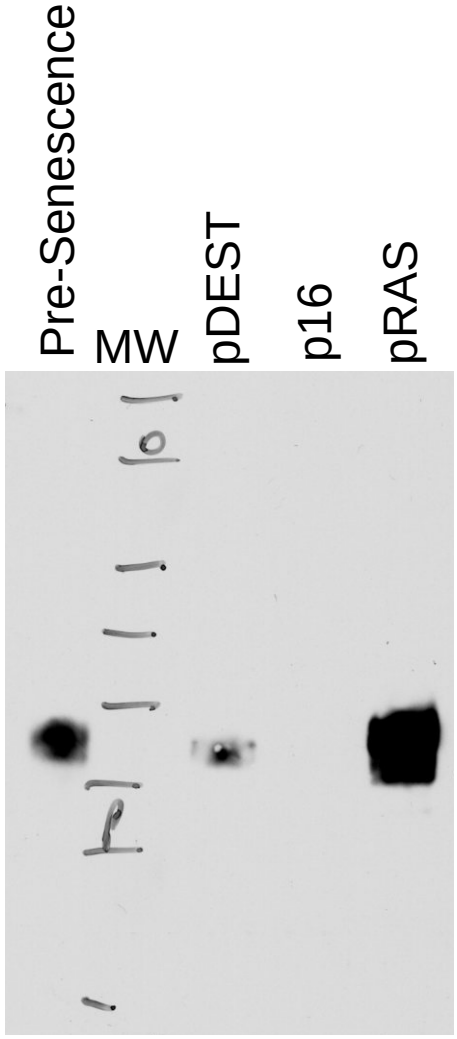

Figure 15

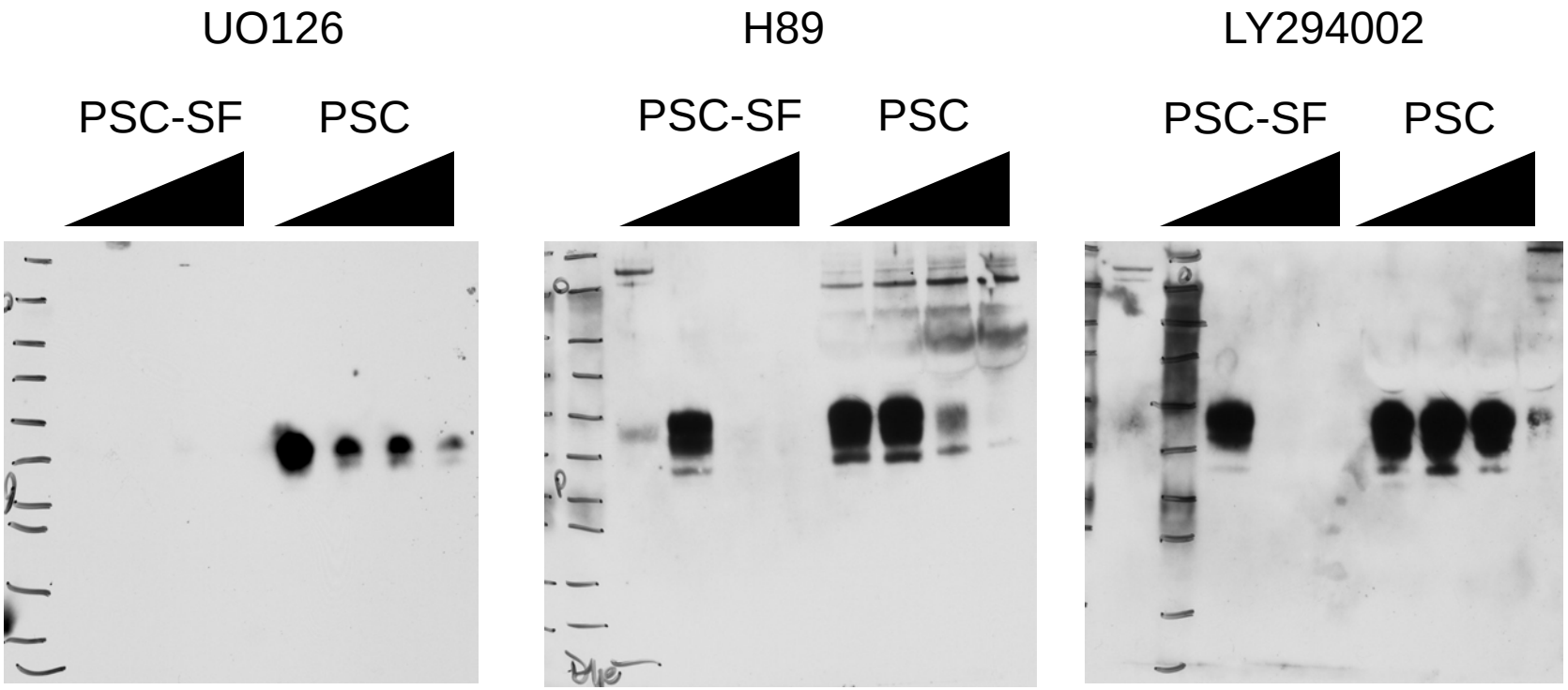

MAPK inhibitor

PKA inhibitor

PI-3K inhibitor

Figure 16

A.

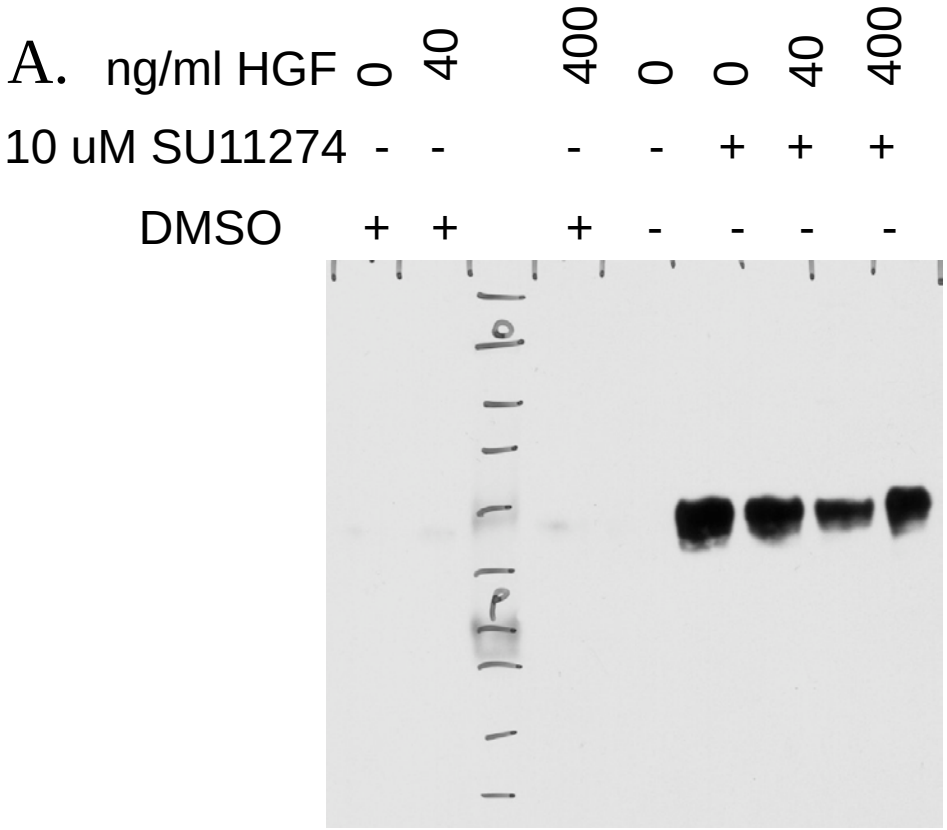
ng/ml HGF 0 40 400 0 0 40 400
10 uM SU11274 - - - - + + +
DMSO + + + - - - -

B.

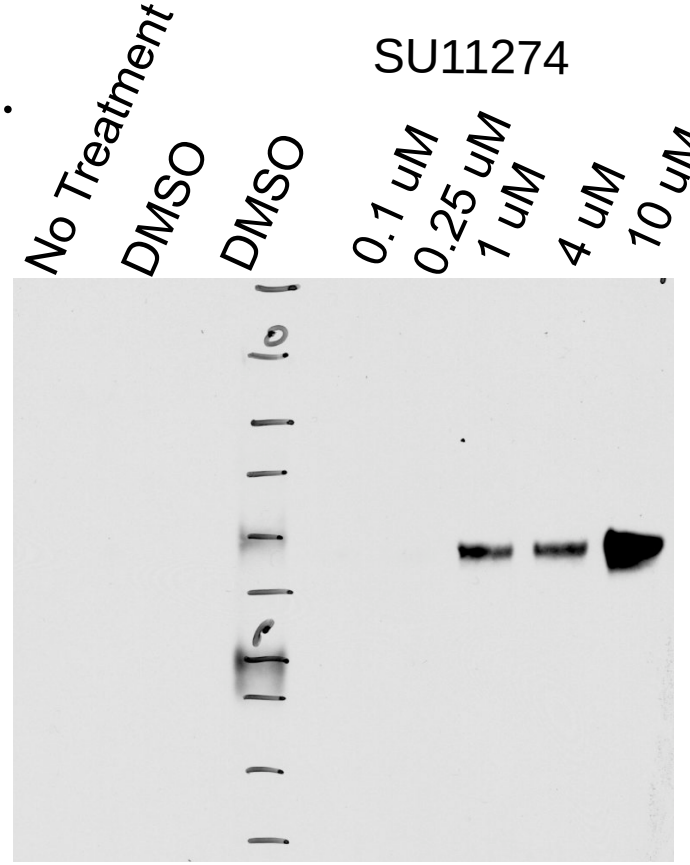
SU11274
No Treatment
DMSO
DMSO
0.1 uM
0.25 uM
1 uM
4 uM
10 uM

Figure 17

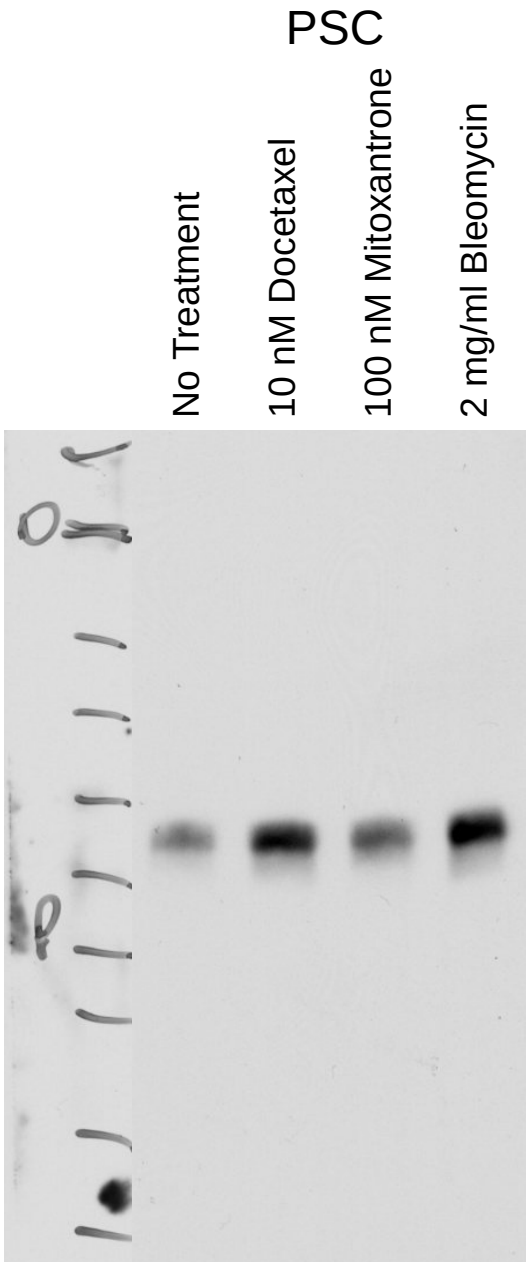
PSC
No Treatment
10 nM Docetaxel
100 nM Mitoxantrone
2 mg/ml Bleomycin

Figure 18

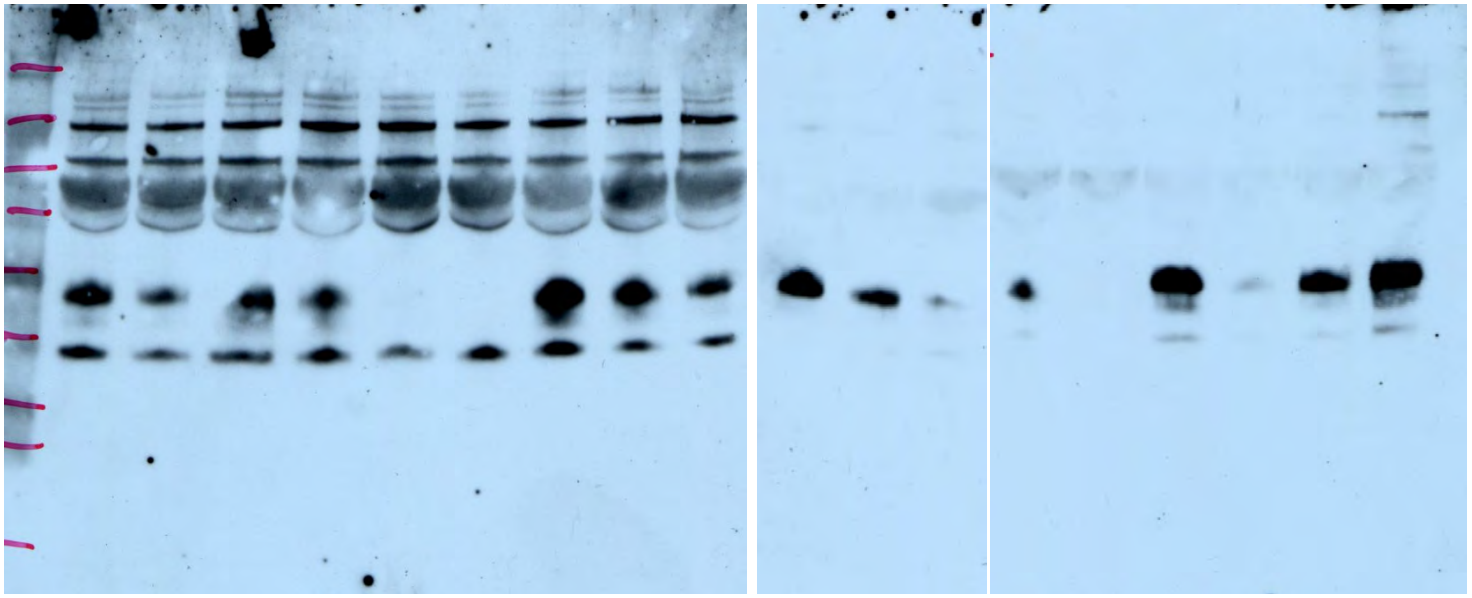

Oxygen	1%	20%	1%	20%	1%	20%	1%	20%	1%	20%	1%	20%	1%	20%	1%	20%	1%	20%
Treatment	none	none	100 mM NaCl	100 mM NaCl	20 mM CaCl2	20 mM CaCl2	10 mM NaPhos	10 mM NaPhos	Mitoxantrone	Mitoxantrone	20 mM MgCl2	20 mM MgCl2	2 mM EGTA	2 mM EGTA	SU11274	SU11274	Docetaxel	Docetaxel

Figure 19. Effects of STC1 modulation on cell proliferation.

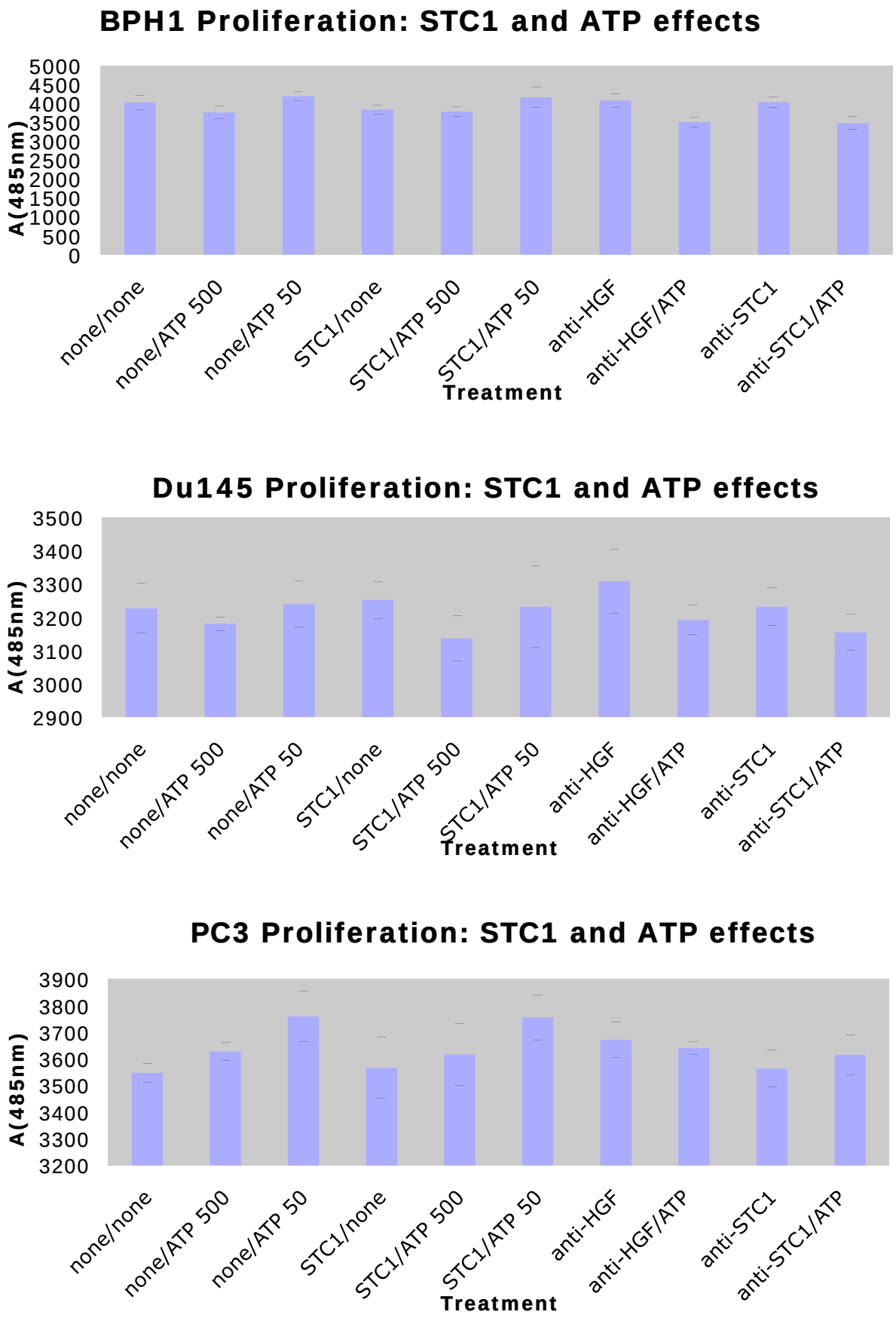

Figure 20. Effects of STC1 modulation on growth in Hypoxia.

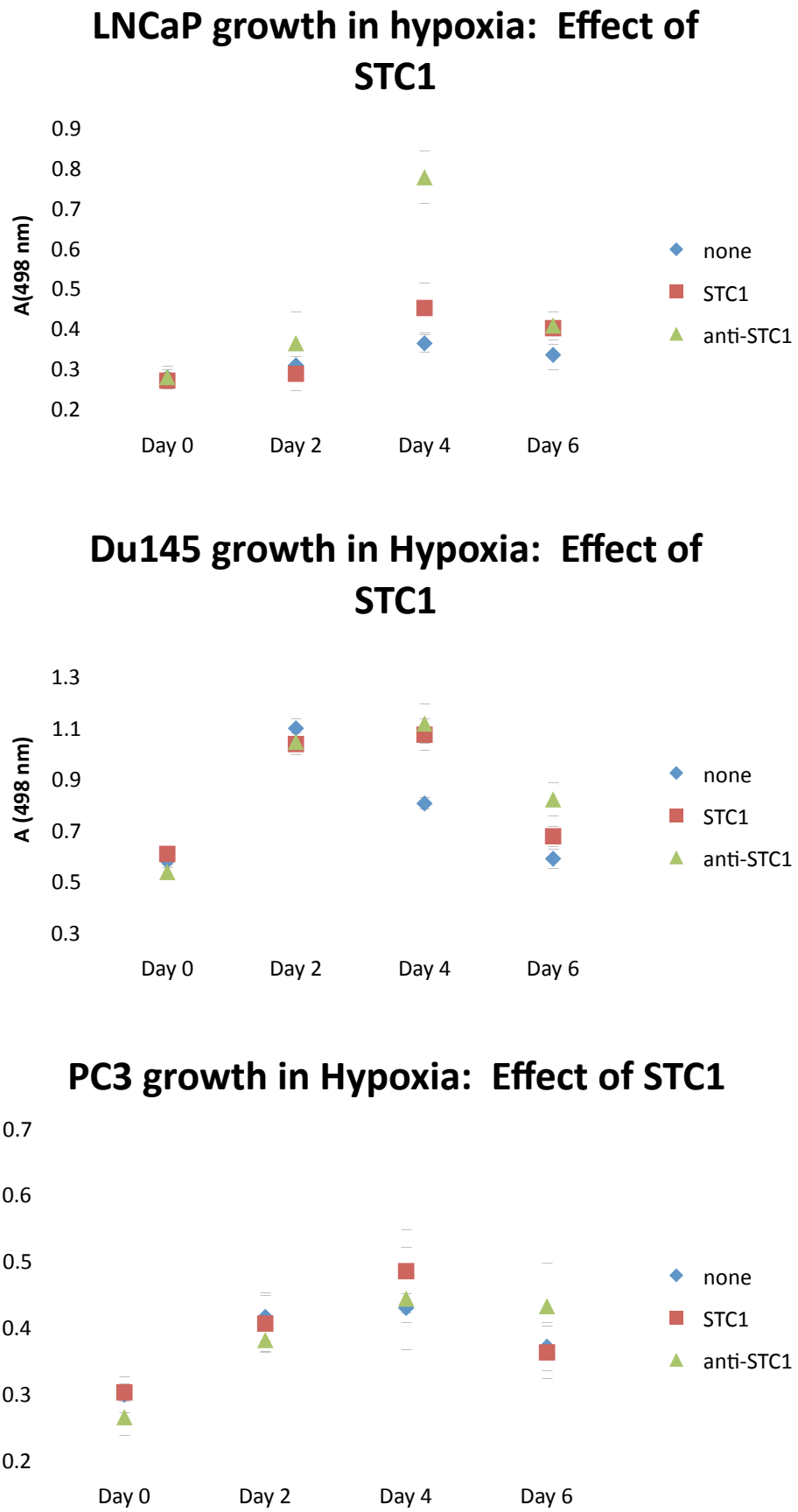

Figure 21. Effects of STC1 modulation on chemotherapy response.

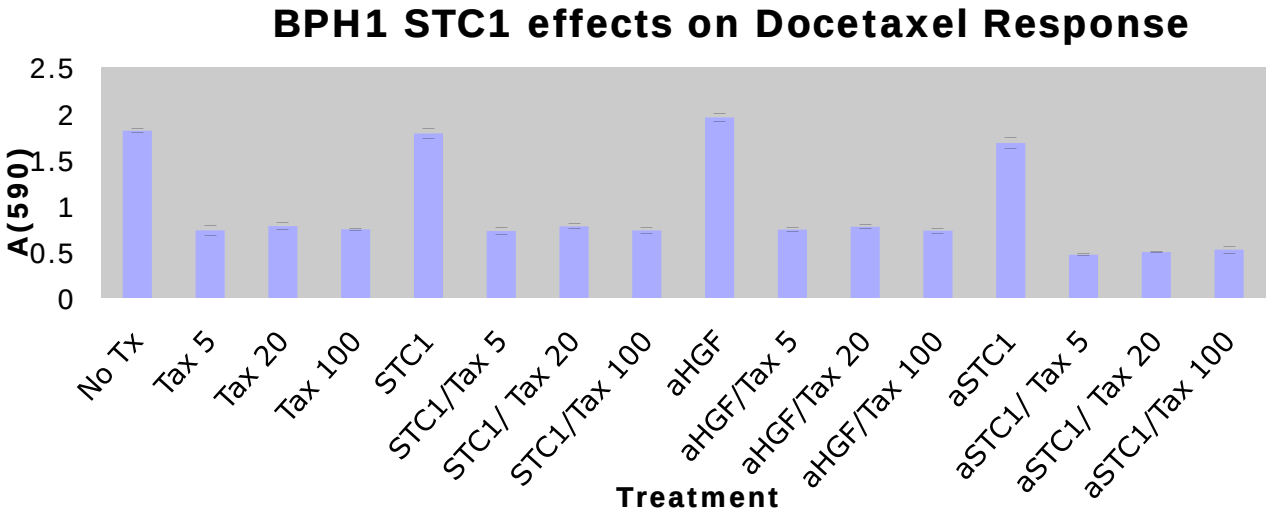

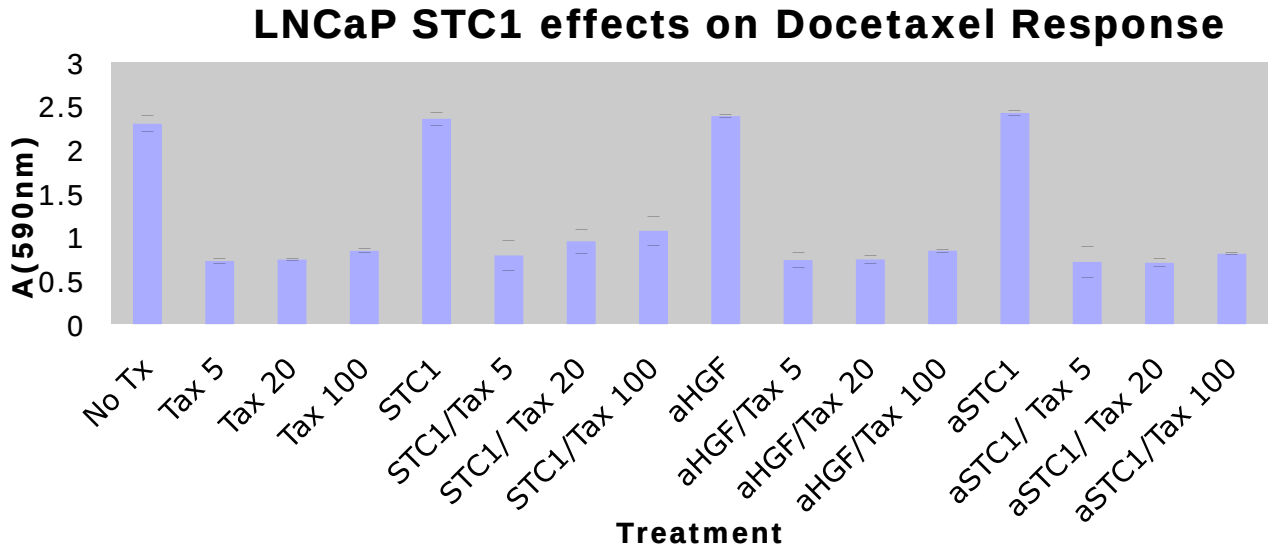

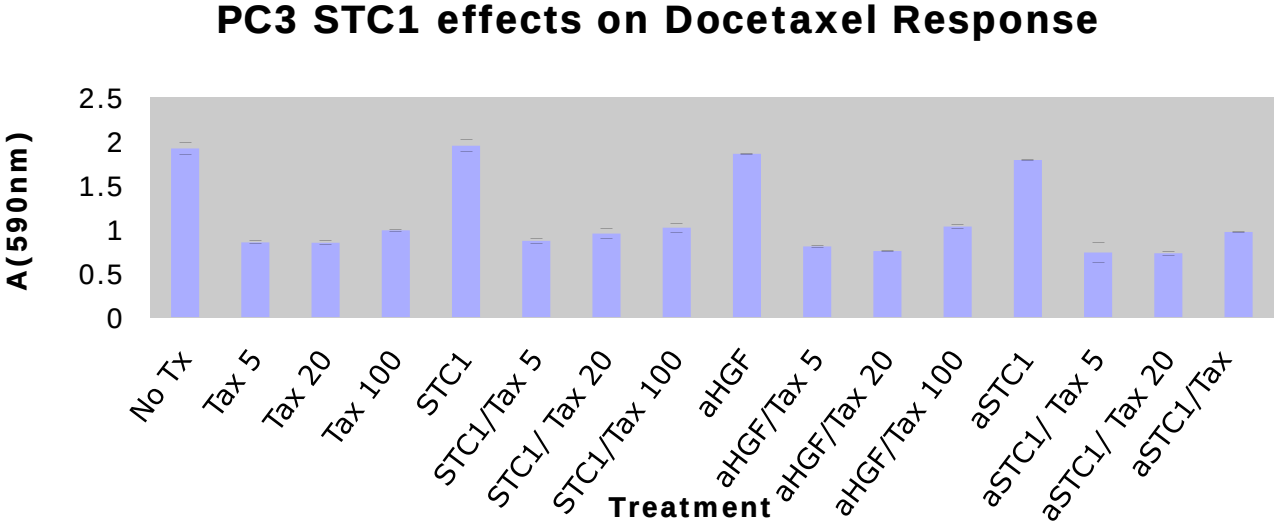

Figure 22. Effects of STC1 modulation on cell migration

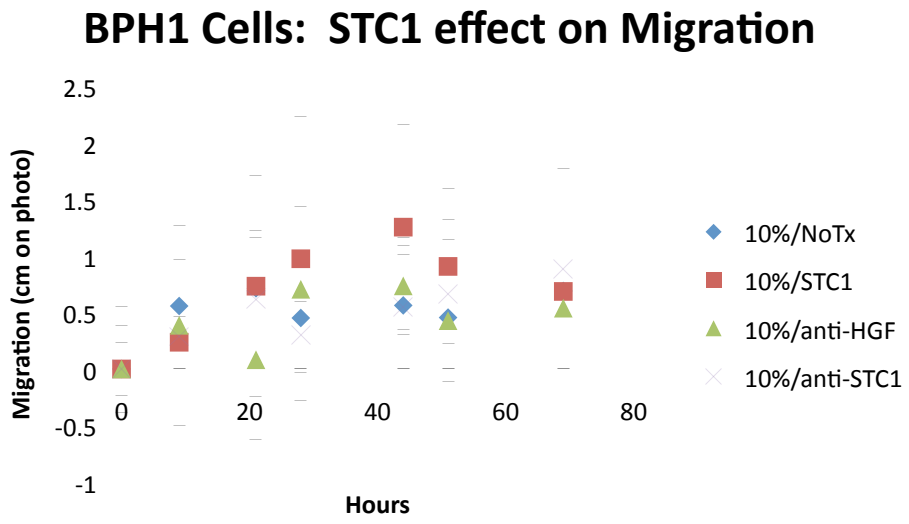

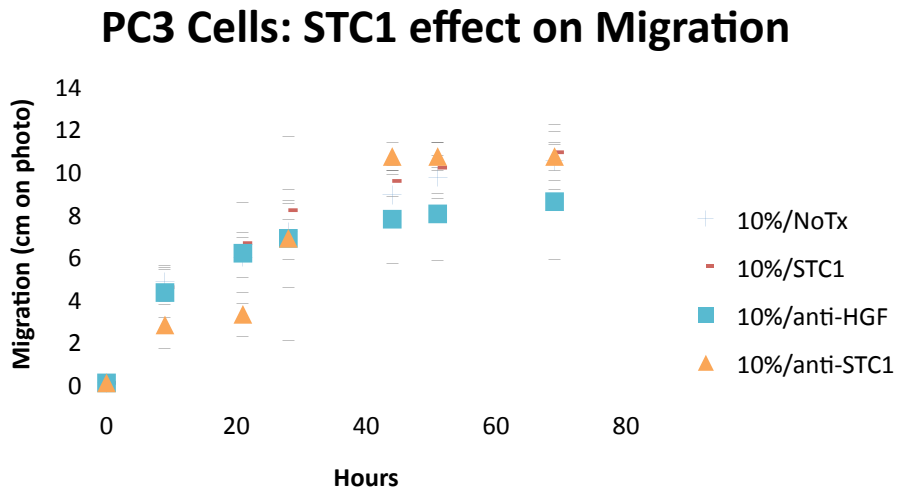

Figure 23. Expression of androgen metabolic genes by PC3 and LNCaP cell lines.

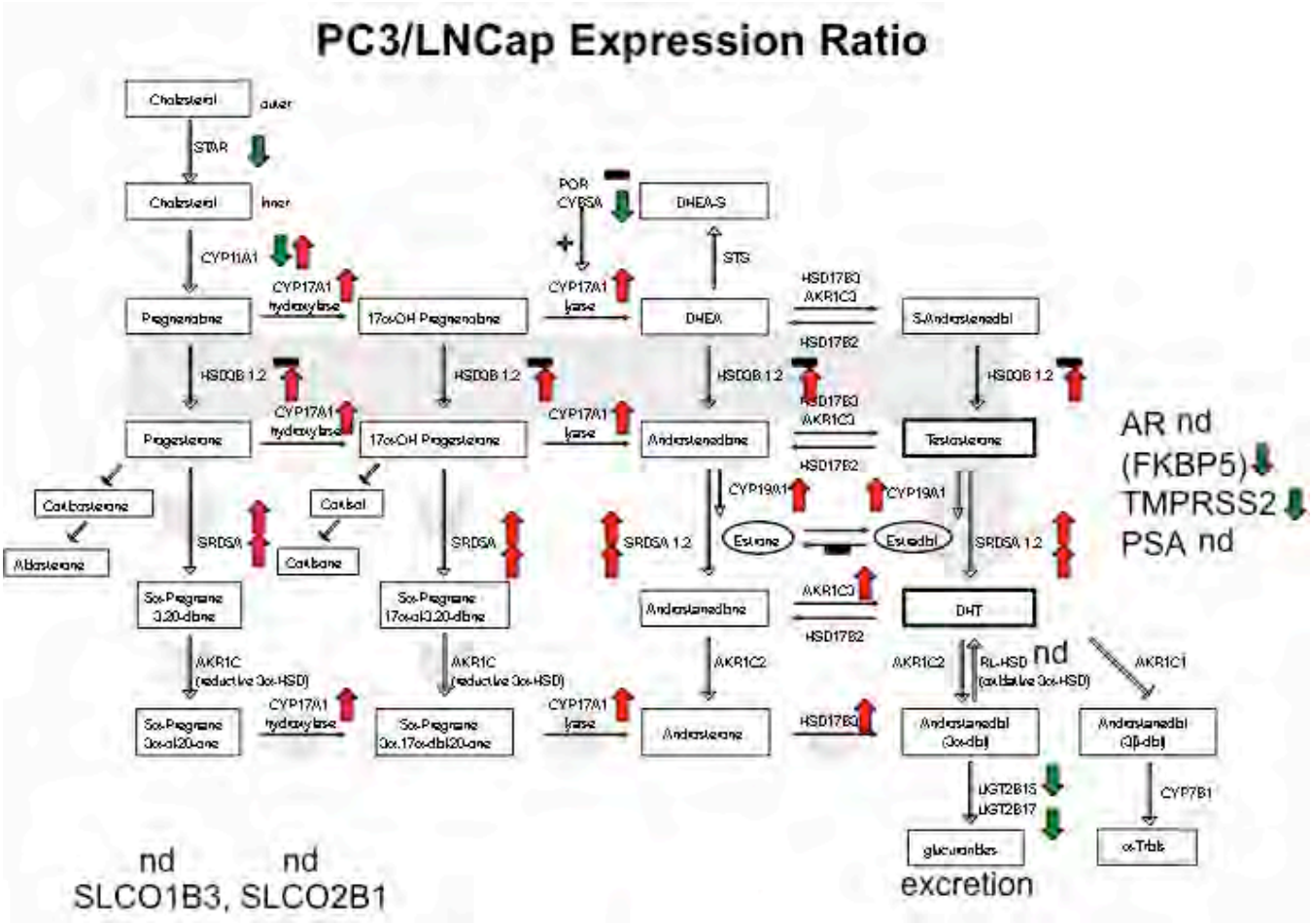

Table 2. Study patient Characteristics

Characteristic	A12 *n*	A12 *Median*	NeoADT *n*	NeoADT *Median*
PSA		**12**		**5.2**
<10	**8**		**11**	
10-20	**4**		**1**	
>20	**6**		**1**	
Gleason Sum		**4+4**		**4+3**
3+4	**3**		**5**	
4+3	**3**		**5**	
4+4	**7**		**1**	
4+5	**5**		**2**	
Clinical T Stage		**T2a**		**T2b**
T1	**4**		**2**	
T2	**8**		**8**	
T3	**6**		**3**	
Body Mass Index		**29.7**		**28**
18.5-24.9	**2**		**3**	
25-29.9	**9**		**7**	
>=30	**7**		**2**	

Table 3. Clinical Pathological and Adverse Event Outcomes

SUMMARY OF PATHOLOGICAL OUTCOMES

- 1 Pathological Complete Response
- 17 pt. Tumor Stage- Similar to Kattan Predictions
- Lymph Node Positivity (6/18)- Similar to Kattan Predictions
- Positive Surgical Margins (4/18)

SUMMARY OF ADVERSE EVENTS

- Probably/Possibly related Grade 1/2 AEs:
  - Hyperglycemia/Diabetes requiring Metformin (2)
  - Asymptomatic Hyperglycemia/Diabetes
  - Skin Rash, Pruritis, Dry Skin
  - Diarrhea
  - Elevated AST
  - Hypertension
  - Increased Lacrimation
  - Blurry vision, Scotomata, Flashing lights
  - Tinnitis
  - Anemia, Thrombocytopenia, Neutropenia
- No Probably/Possibly related Grade 3/4 AEs
  - (Unrelated included peri-operative CVA, post-operative DVT/PE, HTN)

Figure 24. Effects of IGF-1R blockade and hormone therapy on IGF pathway homeostasis

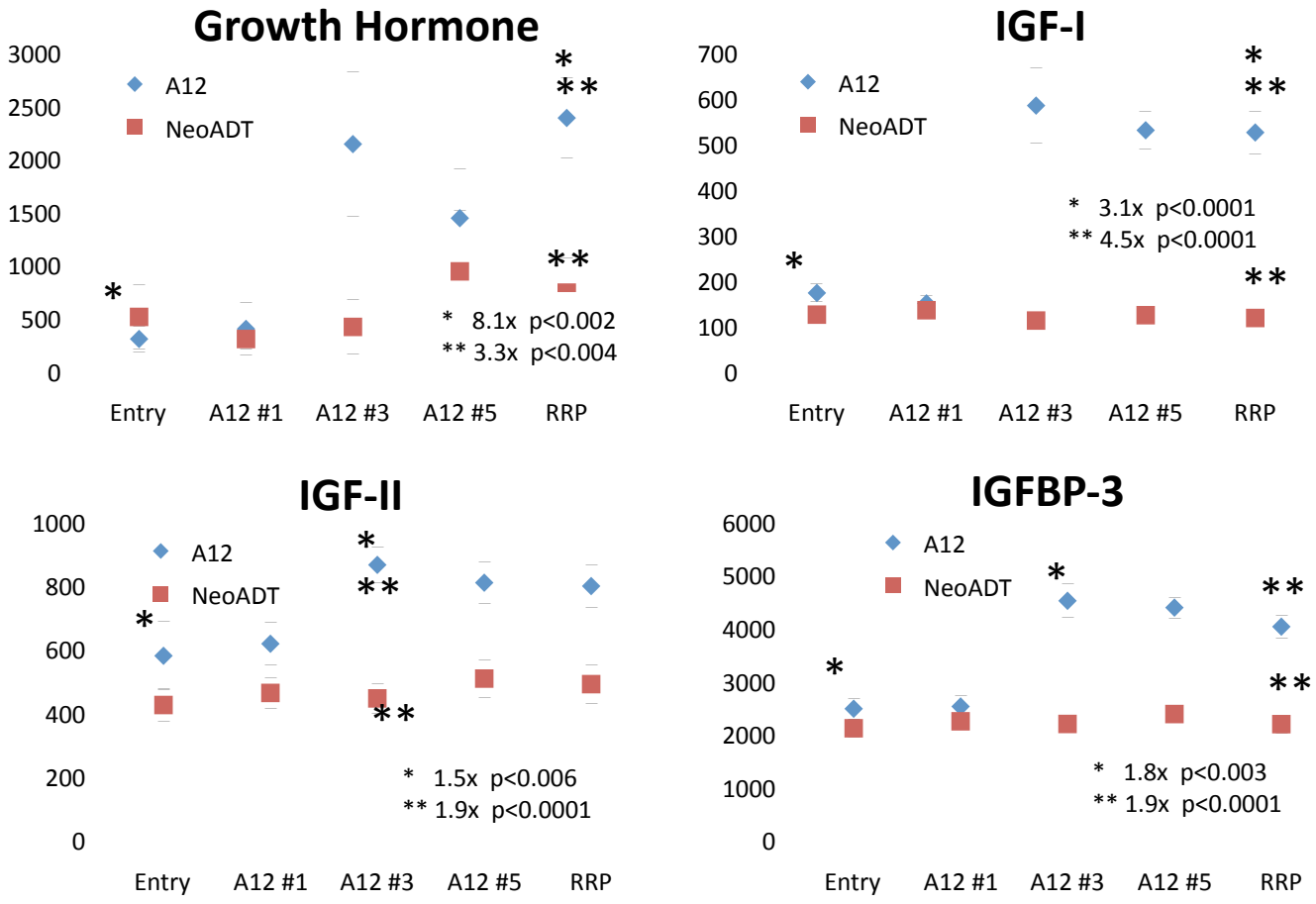

Figure 25. Effects of IGF-1R blockade and hormone therapy on glucose homeostasis and insulin activity

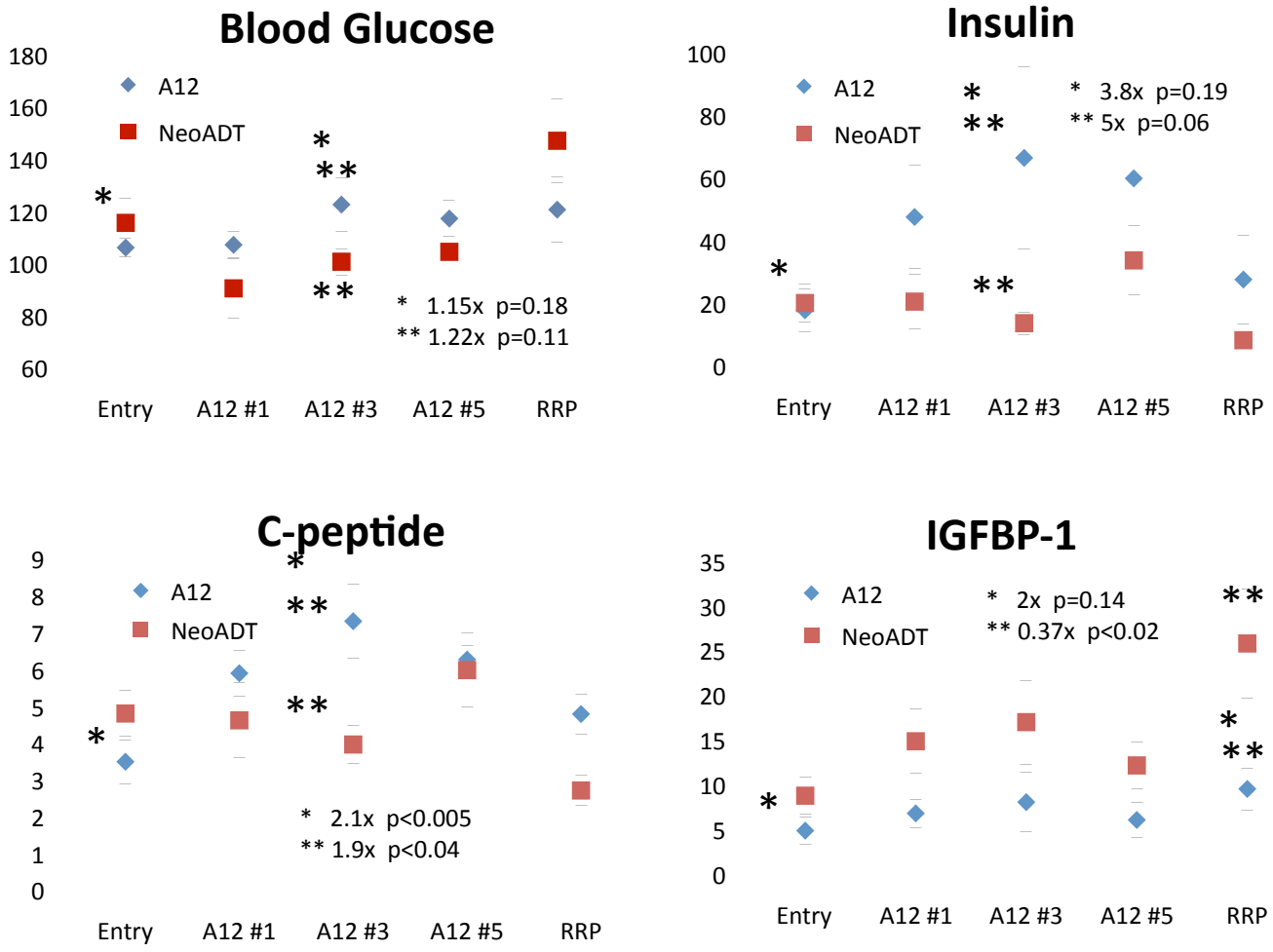

Figure 26. PSA responses and exploratory biomarker correlations

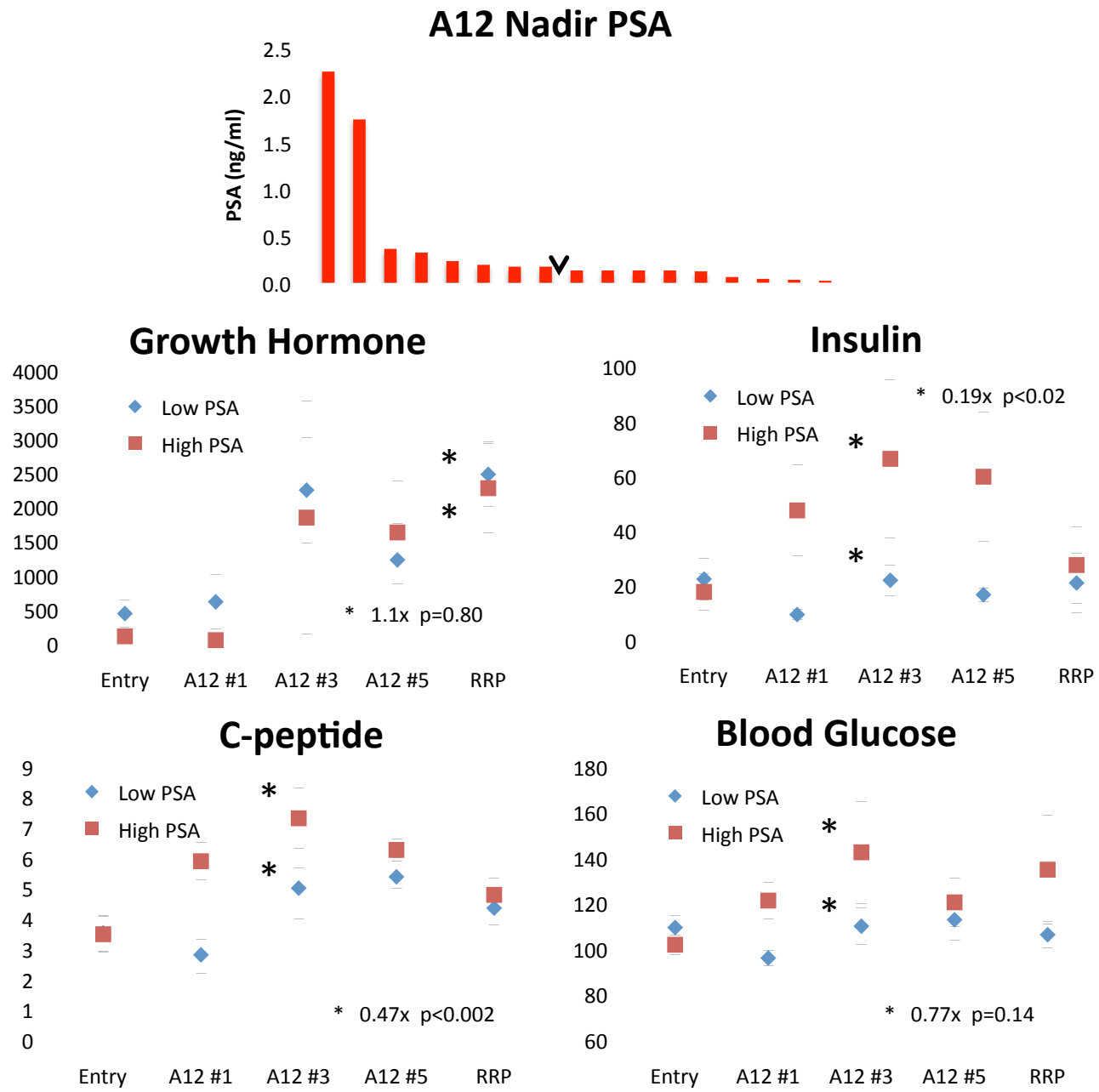

Figure 27. Body Mass Index effects on clinical outcome and biomarkers